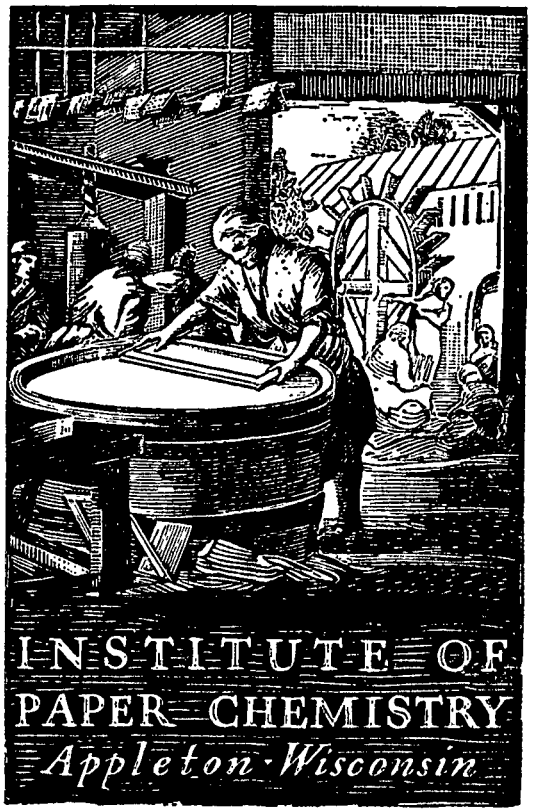

A STUDY OF THE BIAXIAL ENERGY ABSORPTION OF SACK PAPER

Project 2033

Report Forty-one

A Progress Report

to

MULTIWALL SHIPPING SACK PAPER MANUFACTURERS

January 13, 1967

THE INSTITUTE OF PAPER CHEMISTRY

Appleton, Wisconsin

A STUDY OF THE BIAXIAL ENERGY ABSORPTION OF SACK PAPER

Project 2033

Report Forty-one

A Progress Report

to

MULTIWALL SHIPPING SACK PAPER MANUFACTURERS

January 13, 1967

TABLE OF CONTENTS

THE INSTITUTE OF PAPER CHEMISTRY

Appleton, Wisconsin

A STUDY OF THE BIAXIAL ENERGY ABSORPTION OF SACK PAPER

SUMMARY

The impact performance of multiwall sacks depends upon the energy absorption properties in both principal directions of the sack paper. Both directions are involved because the impact forces generated by the contents stress the sack paper in both directions, that is, in biaxial tension. Experiments with sack impact and empirical correlations of sack performance and biaxial paper properties attest to the underlying importance of biaxial stress and strain and hence biaxial energy absorption.

Biaxial tensile properties of paper, such as tensile strength, stretch and energy absorption, should be related to the corresponding properties in uniaxial tension as evaluated in the conventional tensile test, although the relationship has not been determined for paper. The relationship between biaxial and uniaxial tension properties is of great practical importance because the effect of papermaking variables can be most conveniently and effectively studied in terms of the conventional uniaxial tensile tests. The primary objective of this investigation is to determine the relationship between biaxial and uniaxial energy absorption.

A pressure-type biaxial tensile tester was constructed for this investigation. The tester applies pressure to one surface of a circular specimen of sack paper. Pressure on the specimen and distention at the center of the specimen are measured and recorded continuously during the test. Biaxial energy absorption is evaluated from the area beneath the pressure-distention curve, based on the theory of circular membranes and further developed in the Appendices to this report. Distention measurements are also made off-center on two perpendicular meridians

of the specimen for the secondary purpose of studying the deflection behavior of the specimen.

Twelve samples of flat kraft and fourteen samples of extensible kraft sack paper (50-lb., unbleached) from the second fabrication program were evaluated in the biaxial tester. Poisson ratios in the two principal directions were measured by means of a web-straining device; the ratios are required, along with pressure and distention, in the calculation of energy absorption. Among the conclusions reached in this study are the following:

BIAXIAL ENERGY ABSORPTION

Biaxial energy absorption $\Delta\bar{V}$ at the center (most highly stressed region) of the biaxial specimen was calculated from pressure and center distention at rupture and from the Poisson ratios in the two principal directions. These were compared with various combinations of the uniaxial energy absorptions (T.E.A.). Conclusions reached in this phase of the study were the following:

1. Biaxial energy absorption $\Delta\bar{V}$ is greater than the lesser of the two principal T.E.A.'s. This is to be expected. Although the specimen fails at approximately the lesser of M.D. and C.D. stretch, there is a contribution to biaxial energy absorption from the direction of greater stretch.

2. Biaxial energy absorption is less than the sum of the two principal T.E.A.'s because the specimen does not reach the full stretch in the direction of higher stretch.

3. An estimate of biaxial energy absorption denoted by U is obtained by adding the T.E.A. in the direction of lesser stretch (denoted U_1) and the uniaxial energy absorption U_2 in the other principal direction up to a strain level equal to

the lesser principal stretch. This estimate ($\underline{U} = \underline{U}_1 + \underline{U}_2$) underestimated the observed biaxial energy absorption $\Delta\overline{\underline{V}}$ by 24%, on the average. The sense of the disparity is understandable in terms of the Poisson effect in biaxial tension; because of the Poisson effect, biaxial stresses are higher than uniaxial stresses for a given strain, and thus the energy contribution from each principal direction is greater than the corresponding uniaxial energy absorption.

4. The above relationships may be summarized in the following inequalities for flat and extensible sack papers:

Flat: $\text{M.D. T.E.A.} < (\text{M.D. T.E.A.} + \underline{U}_2) < \Delta\overline{\underline{V}} < (\text{M.D. T.E.A.} + \text{C.D. T.E.A.})$

Extensible: $\text{C.D. T.E.A.} < (\text{C.D. T.E.A.} + \underline{U}_2) < \Delta\overline{\underline{V}} < (\text{M.D. T.E.A.} + \text{C.D. T.E.A.})$

where $\underline{U}_2$ is uniaxial energy absorption in the greater stretch direction up to a strain equal to the lesser principal stretch. (This definition of $\underline{U}_2$ applies when the principal strains are in the ratio 1:1, as in the circular biaxial specimen of this investigation.)

5. For purposes of estimation, $\Delta\overline{\underline{V}} = 1.347\ \underline{U}$ for these samples, with an average prediction error of 10%.

6. A reasonable next phase of study is to determine the relationship between biaxial and uniaxial energy absorption at strain ratios other than 1:1. Experimentally this could be accomplished by changing from circular to elliptical specimens. The relationships so obtained can be summarized in the form of energy "interaction" curves. The present study provides three points on the interaction curve.

CORRELATION BETWEEN BIAXIAL ENERGY ABSORPTION AND SACK PERFORMANCE

The correlations between biaxial energy absorption and sack performance were calculated and compared with simple correlations involving combined T.E.A. and multiple correlations with both principal T.E.A.'s. Bearing in mind that biaxial energy absorption was evaluated for only one of the three plies of the multiwall sack, the following conclusions appear warranted:

1. For progressive height face drop, biaxial energy absorption correlated less well than the T.E.A.'s for flat kraft and about equally well for extensible kraft and for the combined data.

2. For butt drop, biaxial energy absorption again correlated less well than the T.E.A.'s for flat kraft and about equally well for extensible. With the combined data, both biaxial energy absorption and combined T.E.A. appeared to be less effective than M.D. and C.D. T.E.A. in multiple correlation. This probably reflects an undue emphasis on M.D. T.E.A. in the biaxial energy absorption (it is obtained at a 1:1 strain ratio) and in combined T.E.A. which gives equal weight to both directions.

3. All of these measures of energy absorption probably suffer from the following deficiencies in so far as repeated sack impact is concerned: (a) they are not fatigue tests; (b) they are performed at slow test rates; and (c) they do not account for the ratio of strains experienced in the sack walls (although the multiple correlations with T.E.A. tend to adjust for this empirically). It is visualized that the biaxial tester can be modified to give a high-speed, fatigue test at arbitrary strain ratio; the fatigue aspect is perhaps the most important of these.

4. It is recommended that further work be undertaken for the purpose of converting the pressure-type biaxial tester to a fatigue tester at the existing 1:1 strain ratio. This type of test would repeatedly stress the sack paper specimen in biaxial tension and thereby progressively dissipate its energy absorption capacity in simulation of what is believed to occur in repeated sack impact. One objective would be to seek improved correlation between sack impact performance and paper quality evaluated by this method.

BEHAVIOR OF SPECIMEN IN BIAXIAL TEST

In some way the pressure-type biaxial tester resembles a Mullen bursting strength tester. A major difference is that the biaxial tester is scaled-up dimensionally about seven times. The objective of the biaxial tester is quite different from the Mullen tester in that interest centers on evaluation of energy absorption rather than bursting pressure. However, a side benefit is that the biaxial tester provides a convenient physical model for study of the fundamental behavior of a bursting strength specimen – a topic of considerable importance in the paper industry.

The pressure-distention behavior and the mode of failure of the biaxial specimen were studied. The results are important to the theory underlying evaluation of biaxial energy absorption and also contribute to a better understanding of the conventional bursting strength test. Among the conclusions arrived at are the following:

1. The bursting pressure of the biaxial specimens (adjusted for diaphragm contribution) ranged from about 3 to 5 p.s.i.g. The bursting pressure for extensible paper was generally slightly greater than for flat papers.

2. The bursting pressures were generally overestimated (by about 19%, on the average) by a well-known equation involving uniaxial tensile strengths and the lesser of the two principal stretches [see Equation (7)]. This result emphasizes that caution must be exercised in inferring biaxial tensile strength from uniaxial tensile strengths because in the general case the latter are not both attained in biaxial tension.

3. The distention at the center of the specimen at failure was in the neighborhood of 0.5 inch for flat kraft and 1.0 inch for extensible kraft. Distention increased with increasing extensibility of the paper, as would be anticipated.

4. The distended shape of the biaxial specimens was found to be very nearly symmetrical about the center point — that is, a surface of revolution — contrary to what might be anticipated with an anisotropic material such as paper. The departure from symmetry (as measured at a point 0.7 of the radius from the center on two perpendicular diameters) was less than 2% of the center distention, which is negligible for most practical purposes. This result considerably fortifies the estimate of biaxial energy absorption which is based on a theory (Hencky-Stevens) that assumes symmetry of the distention surface. The result also indicates that the machine- and cross-direction strains are equal at the center of the specimen.

5. The distention surface for these samples had slightly more curvature than (a) the surface predicted by the Hencky-Stevens theory or (b) a spherical surface as is frequently assumed for the bursting strength test. In terms of the distentions at the aforementioned off-center points, the observed distention surface was about 8% higher than the Hencky-Stevens surface and about 12% higher than a spherical surface (where these percents are based on the center distention). These results indicate that, while the Hencky-Stevens surface is a better approximation

than the spherical surface, it underestimates the deflection of the specimen at points other than the center and the periphery. This probably leads to a small underestimation of the biaxial energy absorption at the center of the specimen.

6. Ninety-seven percent of the flat kraft specimens failed in a manner which may be attributed to exceeding the machine-direction stretch. This is as anticipated because the machine-direction is the direction of lower stretch. The remaining 3% quite likely failed in the same mode, but it is less certain.

7. Eighty percent of the extensible specimens failed in a mode attributable to exceeding the cross-direction stretch. This is in keeping with the lower stretch in the cross-direction of extensible papers. An additional 17% of the specimens quite likely failed in this same mode, leaving only 3% which may have failed in an unexpected manner.

8. The above results indicate that the biaxial specimen generally fails due to exceeding the lesser stretch in the two principal directions of the sheet; this is generally held to be true also of the Mullen bursting strength specimen.

9. Theoretical estimates of failure strain at the center of the biaxial specimens and observed Instron stretch in the lesser of the two principal directions agreed to -9% for flat kraft and +15% for extensible paper, on the average.

10. No difference was found in pressure or distention for the specimen tested "felt"-side up versus wire-side up. Two-sidedness of the sheet does affect the Mullen bursting strength of paperboards, presumably as a result of flexure stresses in the specimen and differential tensile strength across the thickness of the sheet. The relatively lower curvature of the biaxial test specimen and the relatively lower thickness of sack paper evidently minimize flexure stresses and hence any effect of sheet two-sidedness in the biaxial test.

INTRODUCTION

Experiments have shown that during impact the paper in a multiwall sack is stressed in both principal directions, that is, in biaxial tension (1, 2). This indicates that the properties in both principal directions come into play in the impact performance of the sack. The importance of the properties in both directions is also indicated by the empirical correlations of sack performance and paper properties, e.g., tensile energy absorption. The better correlations have involved both machine-direction and cross-direction energy absorption (3-5).

Thwing-Albert impact fatigue, which is a biaxial type of test, has also shown high correlation with sack impact performance. This test property is of limited usefulness to the papermaker because the relationship between Thwing-Albert impact fatigue and the papermaking variables is not known. What is needed is a clearer understanding of the relationship between biaxial tension behavior and the conventional uniaxial test properties such as stretch, energy absorption, and tensile strength – properties which are more fundamental, more universally measured and which can be more readily interpreted in terms of the technology of papermaking.

Experience with materials other than paper indicates that biaxial tension behavior is related to uniaxial properties. Biaxial tensile strength, for example, is found to be related to, but not necessarily equal to, the uniaxial tensile strengths in the principal directions (6-8). It is anticipated that the biaxial stretch and energy absorption of paper differ from, but are related to, the simple uniaxial stretch and T.E.A. in the principal directions of the sheet. Once these relationships are known it should be possible to interpret uniaxial test properties in terms of the biaxial behavior of the paper in a sack. Fully as important, since operation of the paper machine undoubtedly will continue to be governed by consideration of the uniaxial properties of the paper produced on it, the consequences of machine

operation to sack performance promise to be more clearly understood through knowledge of the biaxial-uniaxial relationship.

Study of the relationship between biaxial and uniaxial behavior of sack paper involves development of biaxial test equipment, ideally to include the elements of fatigue and elevated test rates inasmuch as these latter conditions exist in sack impact. It should not be overlooked that the test equipment may provide a useful method for direct evaluation of paper quality which will correlate with sack performance. Thus, a meaningful test method may come as a by-product of the basic investigation of biaxial behavior of paper.

In an earlier study a biaxial test apparatus was constructed which subjected a square specimen of sack paper to in-plane tension in two perpendicular directions, while measuring the total force and elongation in each direction (9). The apparatus proved to be unsatisfactory for the study of the ultimate strength properties of paper because the specimen ruptured prematurely due to stress concentrations near the clamps (10). However, the tester has served well in other contexts such as evaluation of prerupture stiffness and calibration of strain gages in a biaxial stress field (2,11).

Preliminary studies at that time indicated that the disadvantages of a square specimen could be overcome by a different tester design employing lateral pressure against a circular specimen. The present study pursues this approach and a pressure-type tester was constructed for the purpose. This, of course, is the same principle used in the Mullen bursting strength tester. Although the new tester might be viewed as a scaled-up version of the Mullen, the objective is quite different in that interest centers on determination of energy absorption (and possibly also stretch) rather than burst pressure. The scale-up makes these measurements feasible.

It is visualized that the present version of the testing machine can be modified, as interest warrants, to provide (a) a high-speed test, (b) an automated fatigue test, and (c) a variety of strain ratios in the two principal directions of the paper, the latter by changing the specimen shape from circular to elliptical. These test capabilities are of potential interest to future studies directed to the energy absorption and fatigue properties of sack paper and other packaging materials.

The immediate objective of this phase of the investigation is to determine the relationship between biaxial energy absorption and the corresponding uniaxial properties in the principal directions of the sheet. The scope of this report is as follows: following a brief consideration of theory, the biaxial tester and its associated instrumentation are described. The results of initial tests with the apparatus are discussed from the standpoints of the pressure, distention, and nature of failure of the specimen, and correlation with sack performance, as well as the primary objective mentioned above. The theory of the biaxial energy measurement is developed in the appendices to the report.

DESCRIPTION OF PRESSURE-TYPE BIAXIAL TESTER

THEORETICAL CONSIDERATIONS

Application of pressure on one side of a circular specimen of a sheet material (clamped at the periphery) is an effective method of inducing biaxial tensile stresses in the specimen. This method has been in use for many years, of course, in the form of bursting strength testers for paper, paperboard, and films. Interest in the present investigation centers on determining the energy absorbed by the specimen in biaxial tension rather than on the pressure causing rupture as in the conventional bursting strength test.

It may be shown [see Appendix B] that the average energy, $\overline{V}$, (in.-lb./in.^{2}) absorbed by the entire circular specimen is given by the following equation:

$$\overline{V} = 0.5214 \int_0^{w_{o\,max}} p \, dw_o \qquad (1)$$

where w_o is the distention at the center of the specimen, p is the corresponding pressure, and the subscript "max" denotes maximum, that is, rupture of the specimen. Pressure, p, and center distention, w_o, are measurable variables which may be displayed as a graph of p vs. w_o by means of suitable instrumentation. The average energy absorption, $\overline{V}$, is proportional to the area between the curve and the w_o axis. In a practical tester of this type a flexible diaphragm is used to separate the pressure-inducing fluid from the specimen; the energy contribution of the diaphragm may be subtracted from the graphical determination to give the energy absorbed by the specimen.

The average energy absorption, $\overline{V}$, of the specimen is not very useful, however, for comparison with uniaxial energy absorption from the conventional tensile

test for the following reason. The stress distribution is not uniform throughout a circular specimen distended by uniform pressure on one surface. The stress is highest at the center and diminishes as the periphery is approached. This means that the energy absorption also is not uniform; it is highest at the center and least near the clamped periphery. The energy given by Equation (1) is an average over the entire specimen. Accordingly, it is less than the maximum energy absorption at the center which is the value of greatest interest because this is the location of rupture, in general. (Rupture may occur off-center, however, due to local weak spots in the specimen.) Energy absorption at the center of the specimen should be more meaningful for comparison with uniaxial energy absorption evaluated in the conventional tensile test.

The energy absorption at the center of the specimen involves integrals of the form $\int \sigma d\epsilon$ in both principal directions of the sheet, where σ is stress and ϵ is strain. In principle, the strains could be measured at the center of the specimen by means of, say, electrical resistance strain gages and the corresponding stresses could be determined from uniaxial stress-strain curves and knowledge of the Poisson ratios, thereby permitting calculation of energy. This approach would not be convenient for large-scale testing of papers, however, and also would suffer from the uncertainties of measuring strain on a thin sheet material.

For these reasons it was desirable to develop a method of estimating energy absorption at the center of the specimen from measurements of pressure and center distention. This relationship, derived in Appendix B, is as follows:

$$\Delta\bar{V} = 1.1112(1 - \bar{\mu})\int_0^{w_{o_{max}}} p \, dw_o \qquad (2)$$

where $\Delta\overline{V}$ denotes the energy absorption (in.-lb./in.^{2}) per unit of area at the center of the specimen, $\bar{\mu}$ is taken to be the average of the Poisson ratios in the two principal directions of the sheet, and the other symbols are as defined in connection with Equation (1). (A complete listing of symbols is given in Appendix A.)

Equation (2) is based on the Hencky theory for isotropic membranes in the elastic range and further developed by Stevens for stresses in the plastic range (12-14). Two aspects of the theory may be questioned when it is applied to an anisotropic material such as paper. First, the Hencky-Stevens theory leads to a particular shape of the distended membrane which is a surface of revolution, that is, symmetrical about the center point. The surface is quite nearly spherical, differing at most by about 3% in the range of distentions experienced by sack paper. The equation of the surface figures prominently in the development of Equation (2). It may be questioned whether an anisotropic material such as sack paper will distend to a symmetrical surface in this test. Measurements of distention surface of sack paper, presented later in this report, indicate that the surface is indeed symmetrical to within 2%. This is in keeping with an observation attributed to Campbell (15, 16) that the shape of the bulged specimen of paper in the conventional bursting strength test is very nearly spherical. Thus, it appears that the anisotropy of sack paper does not lead to serious complications in the theory underlying Equation (2) in so far as symmetry of the distention surface is concerned.

A second point of concern is the proper combination of machine- and cross-direction Poisson ratios in Equation (2). The isotropic theory, of course, gives no consideration to this question. For lack of information on this point, $\bar{\mu}$ is taken as the average of the Poisson ratios in the two principal directions in this investigation.

Another theoretical relationship of interest to this study is the expression for the strains at the center of the specimen. The strains are equal in both principal directions and are given approximately by the following relationship (12):

$$\epsilon = (1 - \bar{\mu})(w_o/a)^2 \qquad (3)$$

where a is the radius of the circular specimen. The question of the appropriate $\bar{\mu}$ arises again in connection with strain.

It may be remarked in passing that the principal strains at the center of an elliptical specimen are in the ratio (17):

$$\frac{\epsilon_x}{\epsilon_y} = \left(\frac{b}{a}\right)^2 \qquad (4)$$

where a is the semiaxis of the ellipse in the x-direction, and analogously for b and y. Thus, an ellipse leads to relatively higher strain in the short dimension of the specimen (at the center). In terms of the biaxial tester, various ratios of maximum biaxial strain may be achieved by changing the orifice from circular to various elliptical shapes.

PRESSURE AND CLAMPING ASSEMBLY

The biaxial tester is in principle much the same as a Mullen tester; a rubber diaphragm is hydraulically distended, transmitting pressure to the specimen clamped over the diaphragm. It differs in at least three respects from the Model C Mullen tester: (1) It is much larger, having an orifice diameter of 8 inches; (2) the diaphragm (1/16 inch Latex rubber) is about twice as thick; and (3) the diaphragm is mounted so as to be flush with the specimen prior to and throughout the test.

Figure 1 is a photograph showing the biaxial tester and all related equipment as set up to conduct a test. The major components of the system are numbered and identified as follows:

Biaxial Test Apparatus

1. Electric motor – 1/2 hp., 115 v., 1 phase, 1725 r.p.m.
2. Gear reducer – Eberhardt-Denver, Model 16L-DB, 25:1 ratio
3. Drive yoke
4. Pressure cylinder – Nopak, Model A-SS, 6-in. stroke, 4-in. bore
5. Glycerin chamber
6. Pressure gage – Duragage, 15 p.s.i., 1/4 lb./div.
7. Specimen clamp
8. Specimen
9. Frame
10. Base plate

Related Test Components

11. Pressure transducer – Statham, Model PG132TC-15-350, 15 p.s.i.g.
12. Zero adjust and calibration check for pressure transducer
13. Supply voltage for pressure transducer
14. Deflectometer
15. Supply voltage and zero adjust for deflectometers
16. Oscilloscope – Tektronix 502 dual beam
17. Polaroid Land camera attachment

Prior to starting a test the specimen is clamped in place. The clamping surfaces have annular grooves and ridges to hold the specimen securely and eliminate any slippage of the specimen in the clamp. Figure 2 shows a close-up view of the

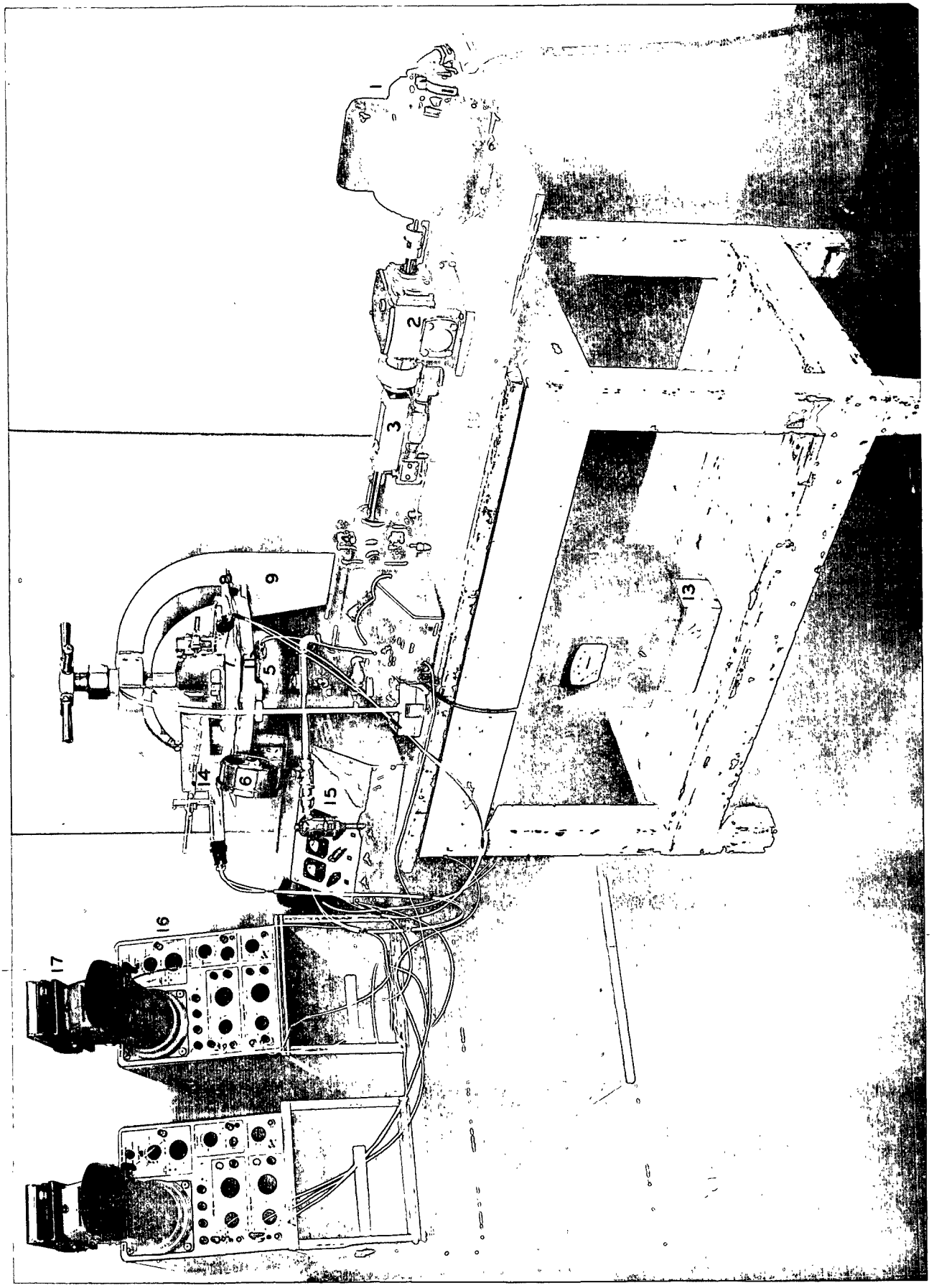

Figure 1. Photograph of Biaxial Tester and Associated Instrumentation

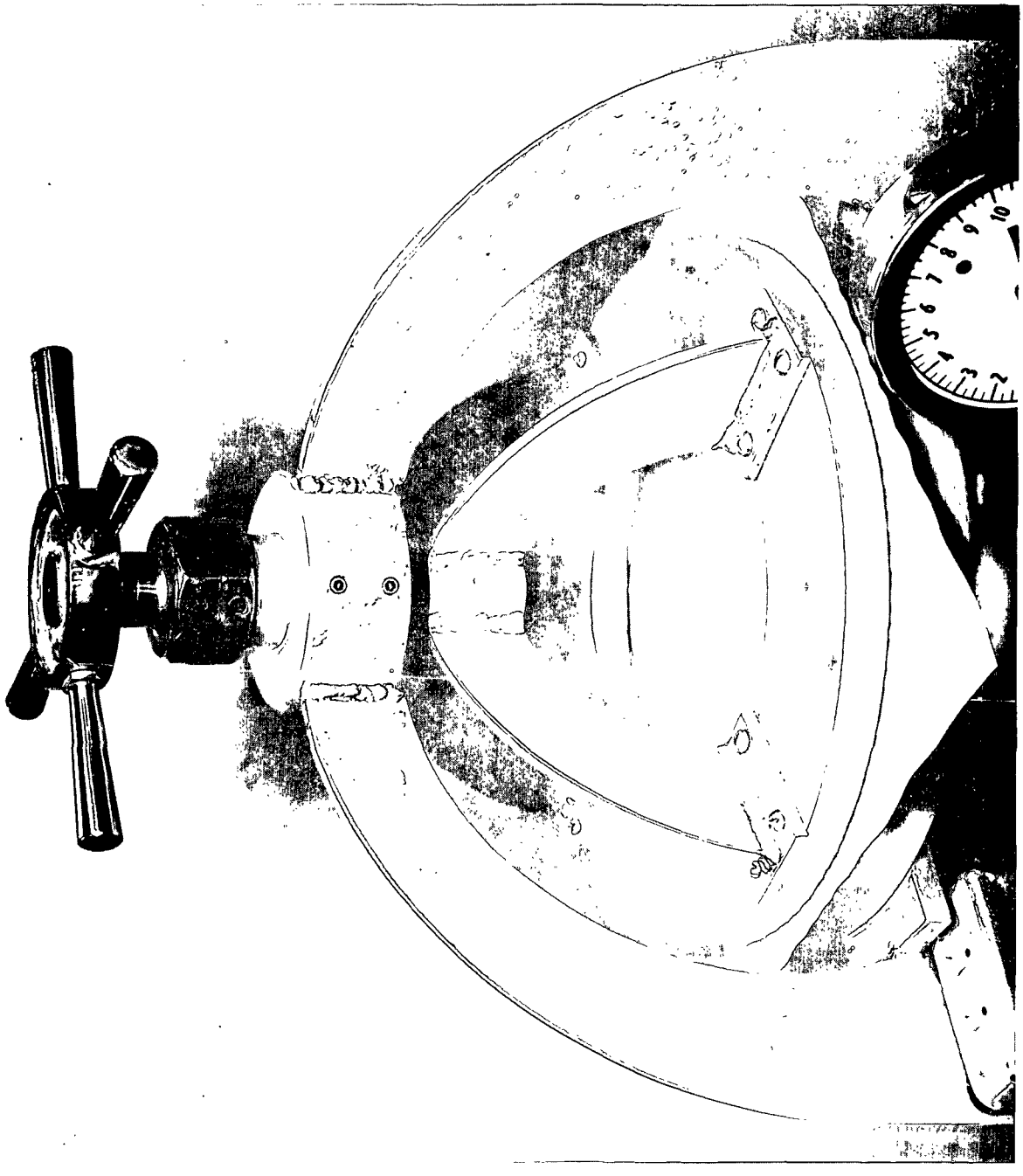

Figure 12. Clamp Assembly of Biaxial Tester

test area of the specimen. In this picture the clamp, test specimen, and orifice area can readily be seen.

When the tester is in operation the pressure applied to the diaphragm and specimen is achieved by the motor moving the drive yoke along a threaded shaft. The drive yoke pushes the piston in the glycerin-filled pressure cylinder forcing more glycerin into the filled glycerin chamber, thereby exerting a pressure on, and causing a distention of, the diaphragm and specimen. After completion of a test the rotation of the motor shaft is reversed, returning the drive yoke and piston to the starting position.

A record of the change in electrical output of the pressure transducer and deflectometers is made by taking Polaroid photographs of the oscilloscope screens during the test operation. The area beneath a curve of central deflection (distention) and pressure is proportional to the biaxial energy absorption.

DEFLECTOMETERS

The measurement of distention of a specimen under test is achieved by converting the linear motion of distention to rotational motion of a lever arm which in turn drives a continuous rotary potentiometer. The voltage output of the potentiometer is proportional to the distention. Three deflectometers of the same design are used to measure distention at the center and on each of two perpendicular meridians of the specimen. Figure 3 is a photograph of the three deflectometers mounted on the clamp assembly of the biaxial tester.

Figure 4 is a photograph of the front and back of the deflectometers. It consists of four major members: (1) the body, (2) the probe (or rider) that contacts the specimen, (3) the lever arm, and (4) the potentiometer.

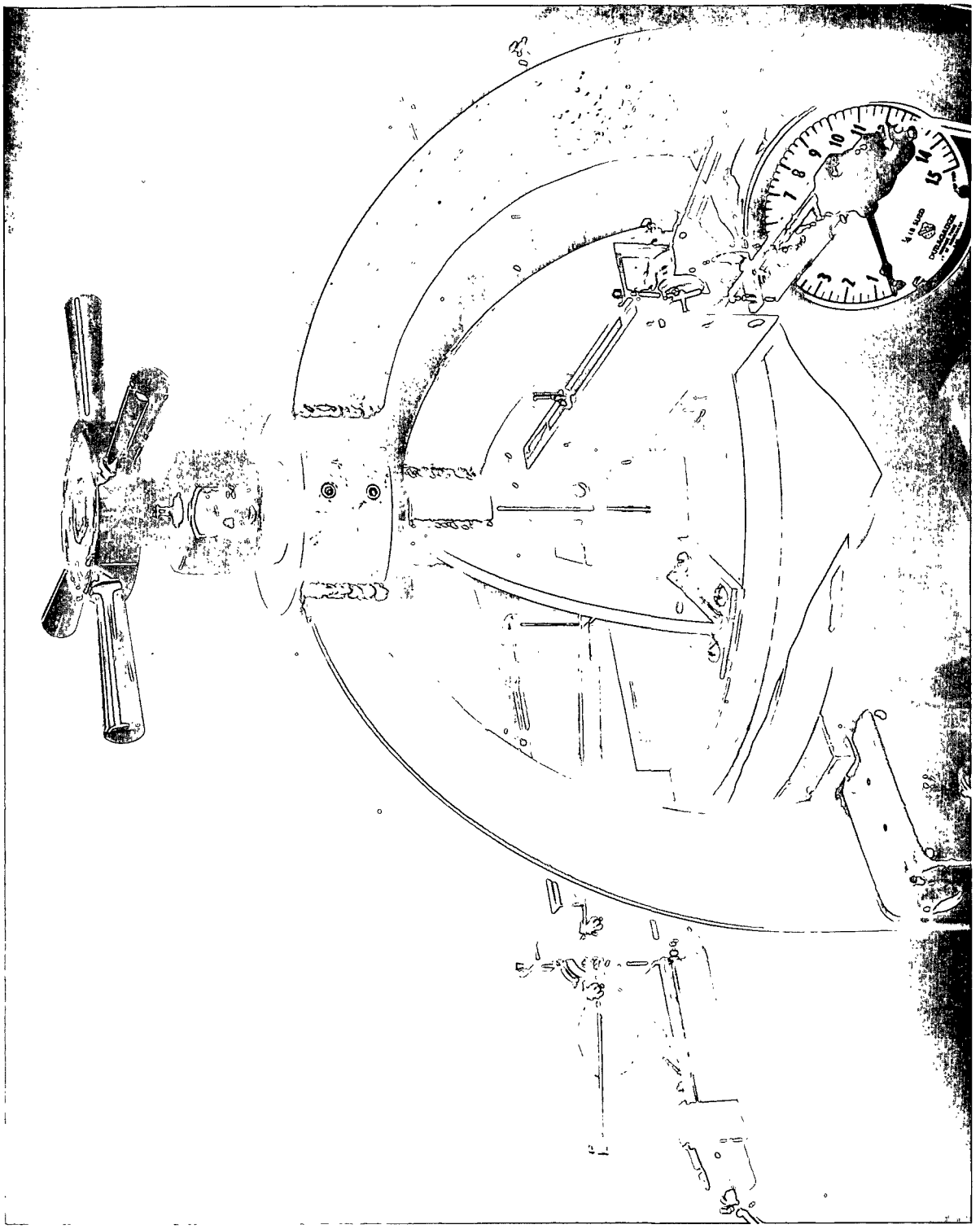

Figure 3. Deflectometers Mounted on Clamp Assembly of Biaxial Tester

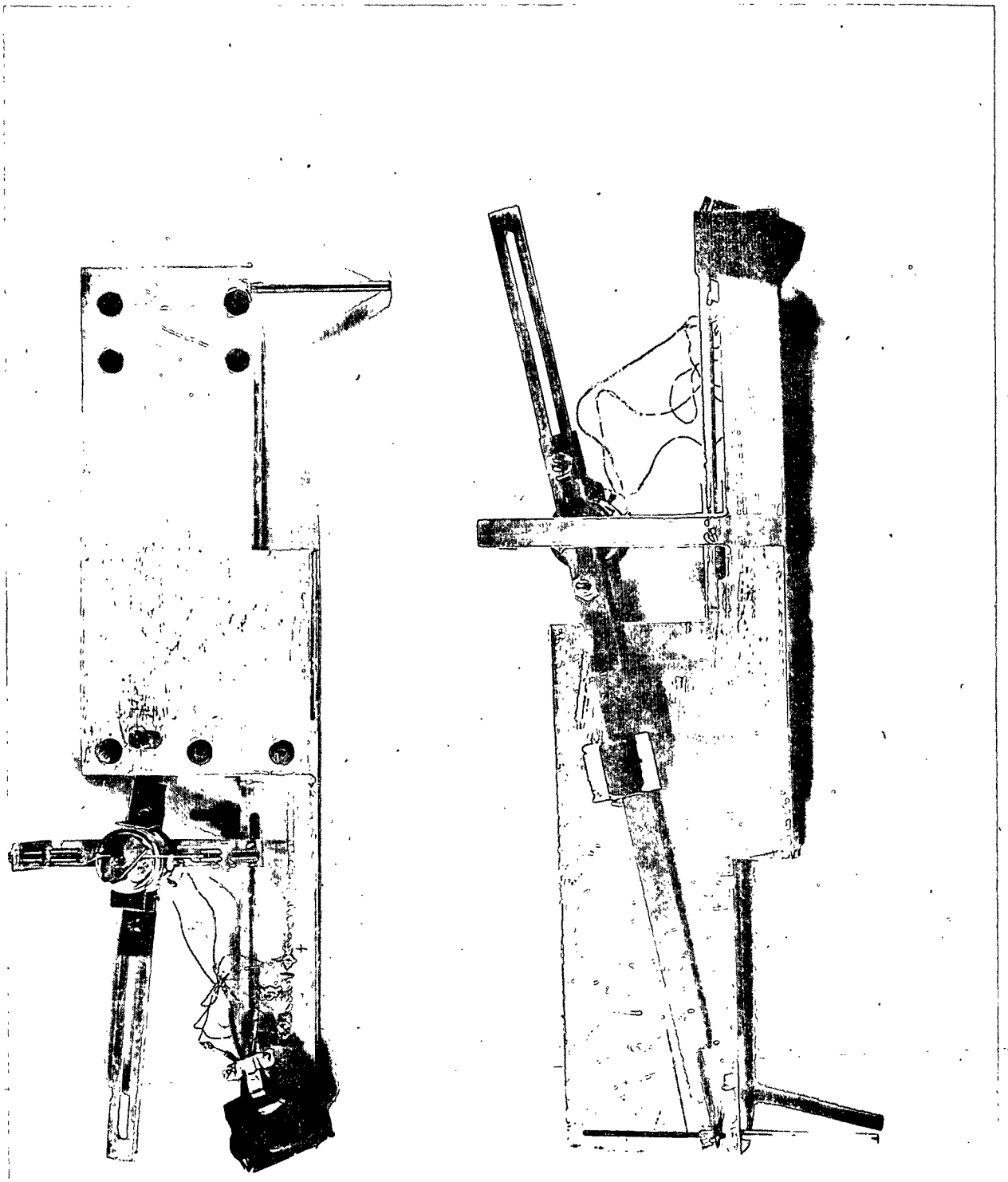

Figure 4. Photograph Showing Construction of a Deflectometer

The body of the deflectometer is constructed of aluminum and is slotted to allow positioning the rider at the desired location on the specimen. At the front vertical edge the body has been drilled to accept the rider and slotted to allow a pin attached to the rider to move vertically without interfering with the movement of the rider. The overall dimensions of the body are 1/2 x 3 x 12 in.

The rider is constructed of a steel rod 1/8 in. in diameter and 2-1/2 in. long. A hole has been drilled in the rider 1/2 in. from the top and perpendicular to the vertical axis to accept a 1/16-in diameter steel pin of 1/2-in. length. This pin provides a contact point for the lever arm and also serves as a stop to keep the rider from falling out of the body of the deflectometer. The pin traverses vertically with the rider in the slot of the body which is provided for this purpose. The function of the rider is to transmit the linear motion of specimen distention to rotational motion of the lever arm. This is accomplished by the pin pushing the lever arm, which rests on it, as the rider is pushed upward by the specimen. The tip of the rider is spherical in the case of two deflectometers which measure the off-center distentions of the specimen.

The lever arm converts vertical movement of the rider to shaft rotation of the potentiometer. The arm is pivoted 6 in. from the rider at 0° rotation. The pivot point is located and fixed by a bushing fitted to a drilled hole in the body. Full-scale rotation of the lever arm is from 9° below the horizontal to 3° above the horizontal. These angles have been kept small so as to minimize the lack of linearity encountered when converting translatory motion to rotary motion. The arm is constructed from aluminum and is 1/8 x 3/8 x 12 in. The arm is slotted behind the pivot point to enable mounting the potentiometer at any location from about 1-1/2 to 4-1/2 in. behind the pivot point. The arm is counterbalanced to make it contact the pin of the rider with minimum pressure on the rider and hence on the specimen.

The potentiometer, which provides an electrical voltage corresponding to the deflection of the specimen, is a Helipot, No. PS273, Model T, 1 K ohm, precision potentiometer. The potentiometer is clamped to the lever arm and located about 1-5/8 in. back of the pivot point. One revolution of the potentiometer shaft corresponds to maximum travel of the rider. The shaft of the potentiometer is rotated, as the lever arm moves, by riding up and down on a string which is double-looped over the shaft and fixed at each end, with a spring fixture at one end to enable maintaining the string taut.

CALIBRATION OF DEFLECTOMETERS

The deflectometers were calibrated to enable converting the voltage output signal of the potentiometer (as displayed on a dual beam oscilloscope) to the vertical displacement of the rider (hence, the distention of diaphragm and specimen). The calibration was performed with the same oscilloscope (and the same beam within the oscilloscope) as was used for testing.

Figure 5 is a photograph of the jig used to calibrate the deflectometers. It consists of a base to which the deflectometer and a Brown & Sharpe depth micrometer were securely mounted. The depth micrometer is used to drive the deflectometer rider through a known distance. The electrical circuit employed with the potentiometer is shown in Fig. 6. Calibration of a deflectometer was accomplished as follows:

1. An input voltage was selected to give approximately 1 cm. deflection of the oscilloscope trace for 1/4 in. of rider travel.

2. The operator turned the barrel of the depth micrometer until the oscilloscope beam traveled 0.4 cm. and then read the micrometer in inches of travel of the rider. (The alternative, which would be less precise, would be to turn the

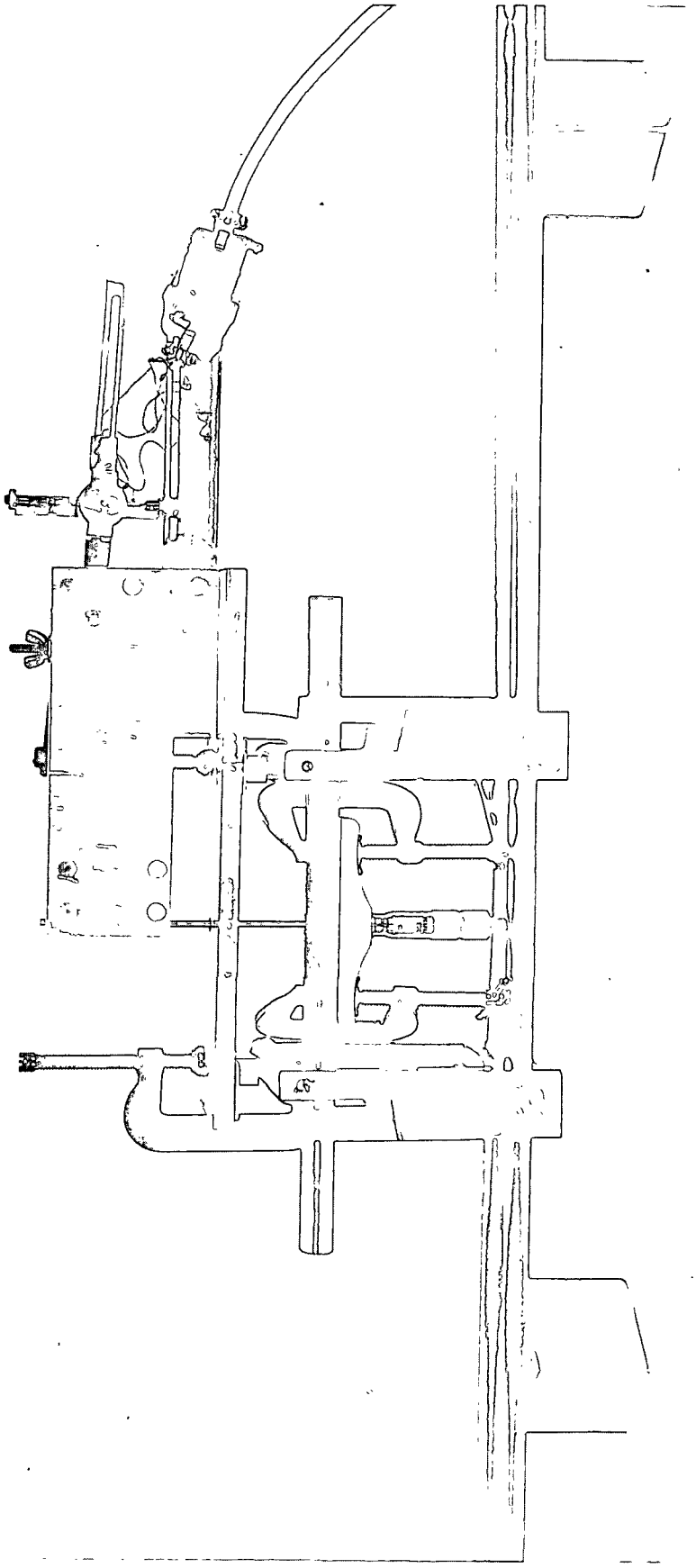

Figure 5. Apparatus for Calibration of Deflectometers

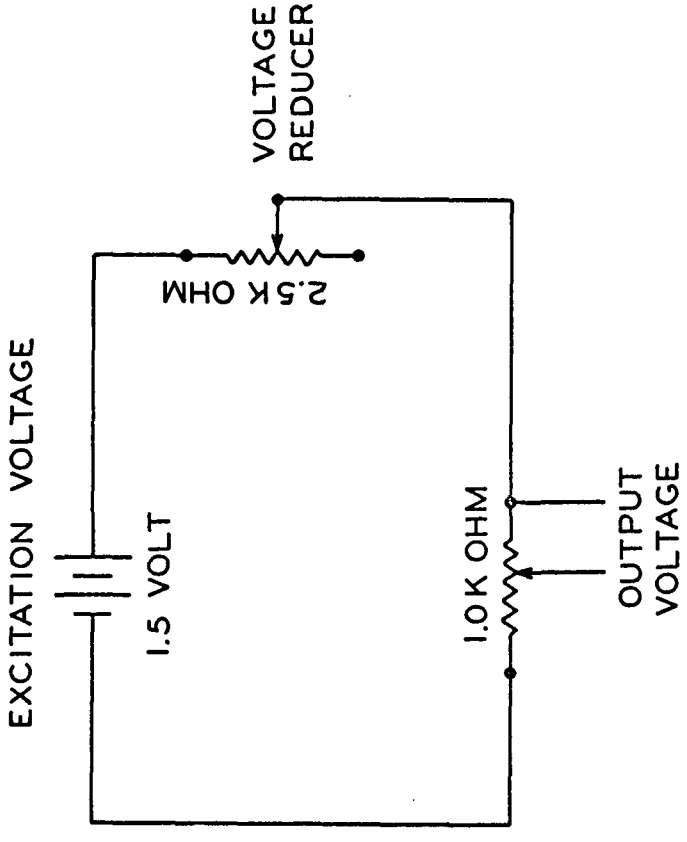

Figure 6. Electrical Circuit for Measurement of Distention

micrometer a given amount, e.g., 0.1 in., and then read the oscilloscope screen in decimal parts of a cm.; this would be a less precise method since the micrometer is marked in one-thousandth inch increments in contrast to the two-tenth centimeter graduations of the oscilloscope screen.) The process was repeated in 0.4-cm. steps until 6 cm. of oscilloscope screen was traversed. Five replications were made for each deflectometer.

3. The average deflection for each increment of screen traverse was obtained and the average deflection was plotted against output in millivolts (the sensitivity setting of the scope in all cases was 1 cm. = 100 mv.). Figure 7 gives the calibration curves for the three deflectometers; the lines were fitted by the method of least squares. The calibration factor (slope of the line) is 0.2439 in. deflection/100 mv. output for Deflectometer No. 1, or equivalently a calibration factor of 1 mv. = 0.002439 in. deflection. An input voltage of 0.63 volt was applied to the potentiometer of Deflectometer No. 1 and thus the calibration factor may also be expressed as 0.003871 in./mv./applied volt or equivalently, 650.8 mv./applied volt/in. The calibration factors of the three deflectometers are summarized in Table I:

TABLE I

DEFLECTOMETER CALIBRATION FACTORS

Deflectometer No.	Calibration Factor in./mv./applied volt	mv./applied volt/in.
1	0.003871	650.8
2	0.003571	571.4
3	0.004026	667.5

MEASUREMENT OF PRESSURE

Measurement of pressure as well as distention is required to determine the biaxial energy absorption of the specimen under test. The pressure measurement

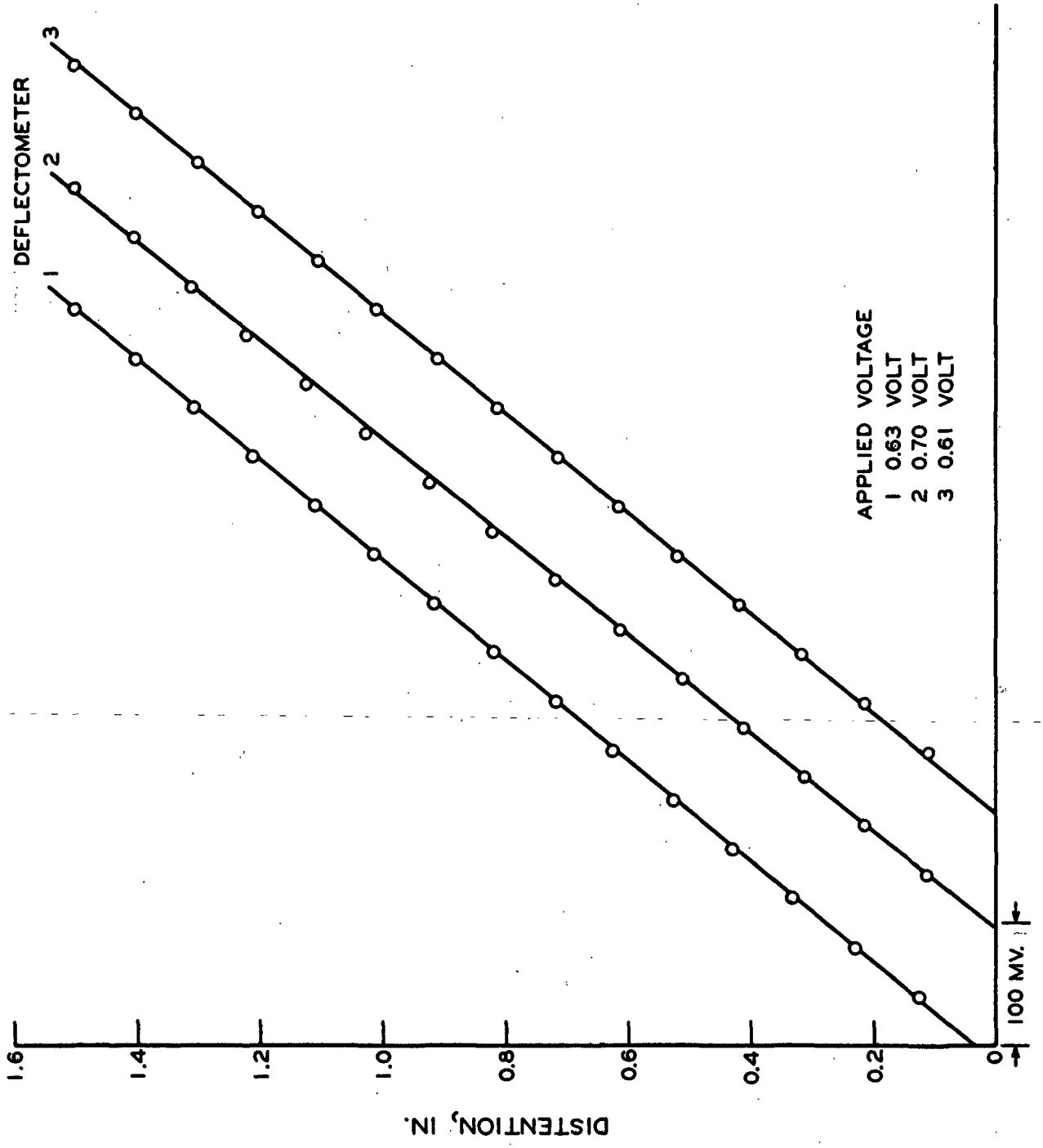

Figure 7. Calibration Curves of Deflectometers

was made using a Statham pressure transducer Model No. PG132TC-15-350 having a range of 0-15 p.s.i.g. The transducer was mounted in the wall of the glycerin pressure chamber of the tester such that the sensitive face of the transducer was flush with the inside wall of the bowl. The calibration factor of the pressure cell, supplied by the manufacturer, was 569.1 microvolt/applied volt/p.s.i.g.

MATERIALS

The materials employed in this study were 26 samples of 50-lb., unbleached kraft sack paper procured in connection with the second fabrication program (4). The specimens were taken from butt rolls corresponding to the outer ply of sacks fabricated in that program. The samples are designated AA to LL for flat kraft and MM to ZZ for extensible kraft.

TEST PROCEDURE

The sack paper samples were preconditioned for at least 24 hours at less than 35% R.H. and 73 ± 3.5°F. and then conditioned for at least 48 hours at 50 ± 2% R.H. and 73 ± 3.5°F. prior to test.

BIAXIAL TESTS

Six specimens from each of the 26 samples of sack paper were tested in the biaxial tester with the "felt"-side uppermost. The deflectometers were positioned at the center of the specimen and at points 2.8 in. from the center on two perpendicular meridians, as illustrated in Fig. 8. These off-center points were selected on the grounds that the difference between the Hencky-Stevens theoretical deflection surface and a spherical deflection surface is greatest at approximately $r/a = 2.8/4.0 = 0.7$ [see Fig. 23, Appendix B]; thus, 2.8 in. is the most sensitive location for discriminating between distention surfaces. The machine direction of

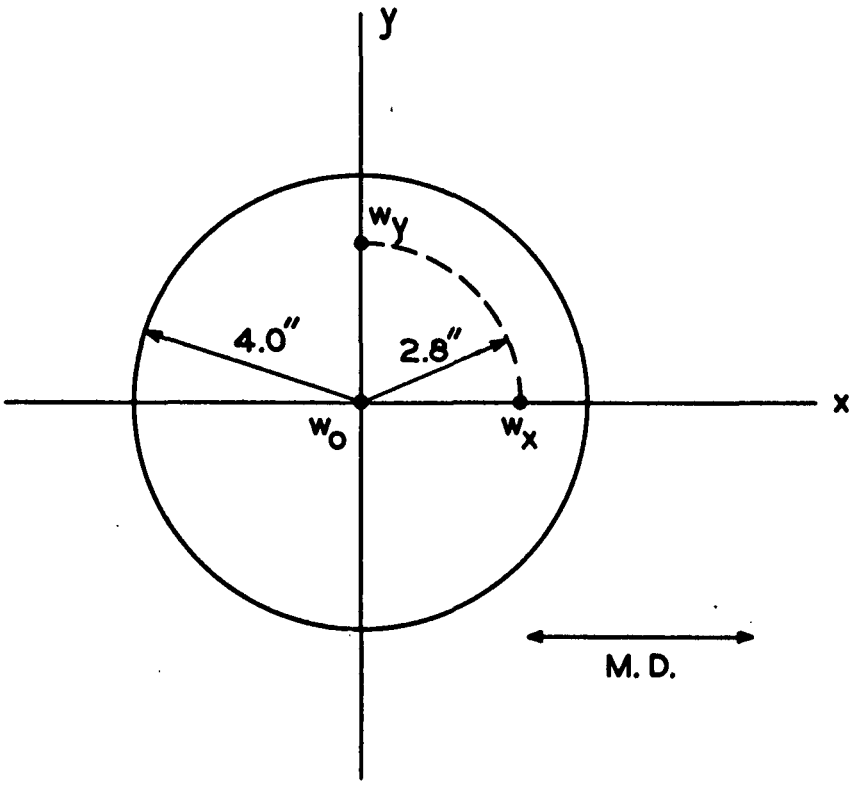

Figure 8. Location of Distention Measurements on Sack Paper Specimens

successive specimens in a sample of six was rotated 90° relative to the clamps of the tester to average out any possible systematic effects attributable to orientation in the tester.

Pressure, p, and center distention, w_o, were displayed as y-x variables on one dual-beam Tektronix 502 oscilloscope. This provided a continuous curve from zero to rupture; the area beneath the curve is proportional to energy absorption, as discussed in THEORETICAL CONSIDERATIONS. A second dual-beam oscilloscope (same model) displayed the off-center distentions vs. center distention, providing continuous curves of w_x vs. w_o and w_y vs. w_o, where w_x is the distention on the machine-direction meridian 2.8 in. from the center, and w_y is the distention on the cross-direction meridian at the same distance from the center. Polaroid photographs of the oscilloscope curves were taken for purposes of subsequent data analysis.

The contribution of the rubber diaphragm was measured 16 times during the testing. A determination consisted of recording pressure vs. center distention of the diaphragm alone. There was no evidence of systematic change in diaphragm contribution during the course of testing.

A spot-check calibration of the deflectometers at the conclusion of the test program was in satisfactory agreement with the calibration reported above.

Subsequently, a brief study was carried out to determine whether there was a detectable effect in placing the wire-side of the specimen up vs. down in the test machine. Five specimens were tested in each orientation from one sample of flat, 6 and 12% extensible kraft paper. The test procedure was as described above except that pressure and the three distentions were recorded as functions of time with an oscillograph recorder.

It may be remarked that the duration of the biaxial test ranges from about 15 sec. for flat kraft to about 30 sec. for 12% extensible kraft paper. This places the biaxial test on approximately the same time scale as the conventional uniaxial tensile test.

POISSON RATIO

The Poisson ratio in each principal direction of the paper was measured for purposes of calculating energy absorption and strain by Equations (2) and (3). Measurements needed for calculating Poisson ratio were made on a 15-in. long by 15-in. wide sheet of the sack paper which was strained in a motor-driven web strainer, as shown in Fig. 9. The paper is clamped at two opposite edges and strained by the rotation of the motor-driven barrel. The specimen is free to contract in the lateral direction, except at the clamps.

The procedure for measuring Poisson ratio was as follows: A 10-in. gage length was marked with pencil on the paper specimen in the direction of straining and in the lateral direction. The gage marks correspond to the four end points of a plus (+) sign centered on the specimen. The gage lengths were measured with a steel scale graduated to 0.01 in. and estimated with the aid of a magnifying glass to the nearest 0.005 in. Measurements were made initially with just perceptible strain in the specimen and at subsequent increments of strain until the specimen ruptured. The strain increments were as follows:

flat kraft	0.010 in.
6% extensible	0.050 in.
9% extensible	0.075 in.
12% extensible	0.100 in.

Five specimens were strained in each principal direction of each of the 26 samples of sack paper.

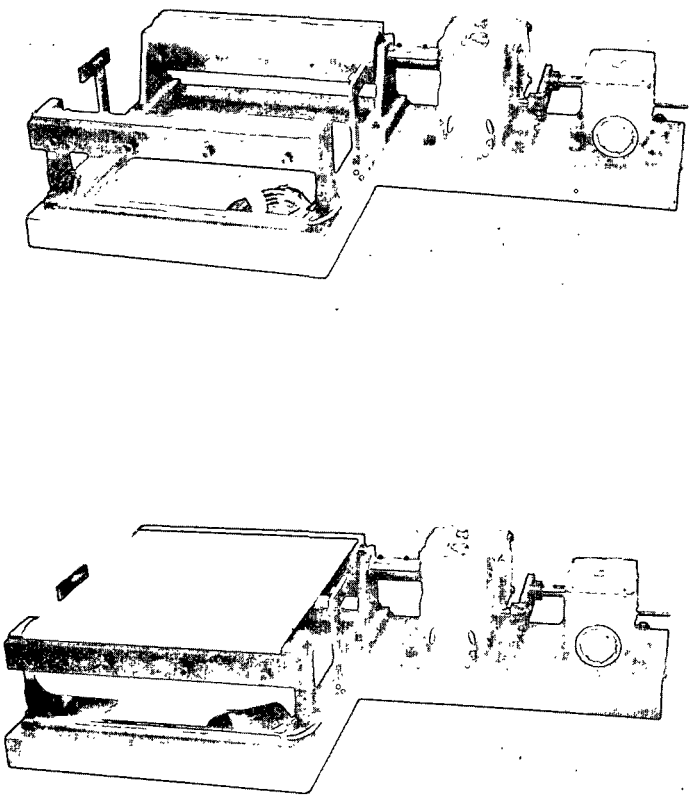

Figure 9. Web Strainer Used in Determination of Poisson Ratio

Poisson's ratio μ was calculated as follows:

$$\mu = \frac{(y_o - y)/y_o}{(x - x_o)/x_o} \qquad (5)$$

where x is the measured gage length in the direction of straining, y is the gage length in the lateral direction, and subscript o refers to the initial measurement.

Poisson ratios near rupture are needed for estimation of biaxial rupture energy. Graphs of the estimates of Poisson ratio vs. strain indicated that the ratio was reasonably constant from about 50% of ultimate strain to rupture. This is also the region of best precision of the measurements. It was decided arbitrarily, therefore, to average the individual determinations of the ratio over the latter half of the strain region. Considering all five specimens of a given type, the number of determinations entering the average ranged from 23 to 62.

CALCULATION OF ENERGY ABSORPTION

A typical oscilloscope record of pressure vs. distention is shown in Fig. 10. The photograph on the left is pressure p vs. center distention, w_o. The photograph on the right has w_x vs. w_o in the upper trace and w_y vs. w_o in the lower trace, with polarities as indicated. The broad bands about the latter curves result from a "halo" centered on each beam – a peculiarity of this particular cathode ray tube. It may be noted that the off-center distentions w_x and w_y are approximately proportional to the center distention w_o, in keeping with the Hencky-Stevens theory [see Equation (11), Appendix B].

The following procedure was employed to evaluate energy absorption at the center of the specimen according to Equation (2). A 35-mm. negative was made of each Polaroid photograph of the oscilloscope trace. The negative was projected in a Microfilm reader to give suitable magnification. A tracing was made of the

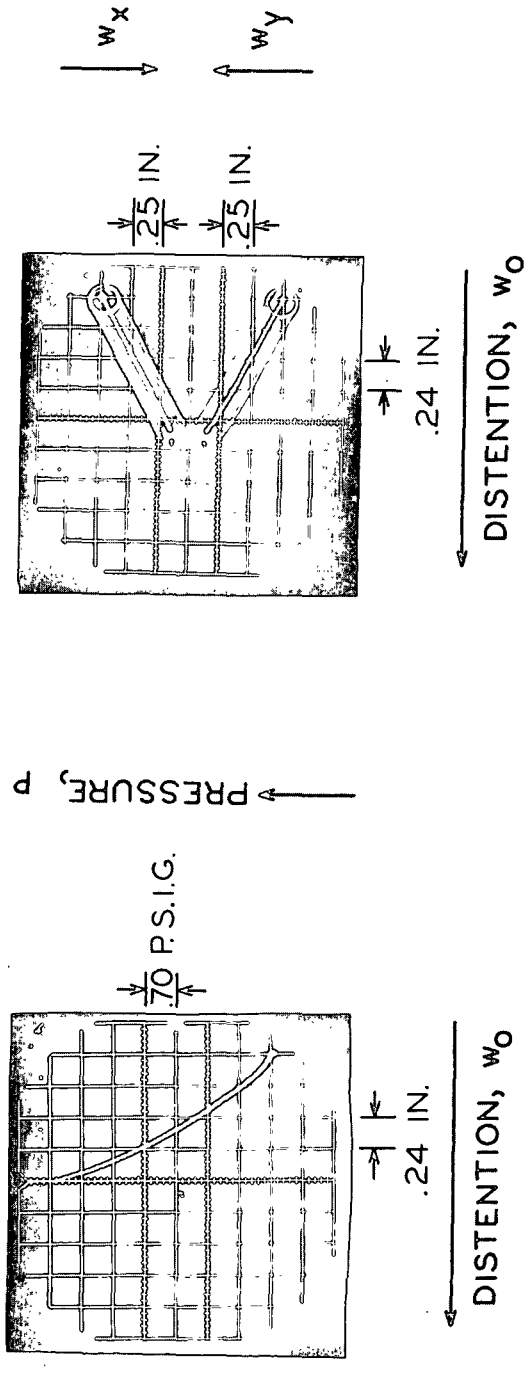

Figure 10. Representative Experimental Curves of Pressure and Distention

pressure-distention curve and of a reference rectangle comprised of a number of squares of the grid enclosing the curve (the latter to establish the scale factor). The area under the curve was measured by means of a planimeter. Energy absorption (of the specimen and diaphragm combined) was calculated as follows:

$$\Delta\bar{V} = 1.1112(1 - \bar{\mu})PQSA/M \qquad (6)$$

where $\Delta\bar{V}$ = energy absorption per unit area at center of specimen, in.-lb./in.^{2}

$\bar{\mu}$ = average of M.D. and C.D. Poisson ratios, dimensionless

P = pressure transducer calibration factor, lb./in.^{2}/scope cm.

Q = deflectometer calibration factor, in./scope cm.

S = area of reference rectangle on oscilloscope, cm.^{2}

M = area of reference rectangle on tracing, in.^{2}

A = area under pressure-distention curve on tracing, in.^{2}

An analogous calculation was made for the energy contribution of the rubber diaphragm (in the absence of a specimen), based on an average pressure-distention curve representing 16 determinations during the course of the test program. The energy absorption of the specimen was then obtained by subtracting the diaphragm contribution from the total energy. The average percent contribution of the diaphragm to the total energy is shown in Table II.

TABLE II

CONTRIBUTION OF DIAPHRAGM TO TOTAL BIAXIAL ENERGY

Type of Paper	Diaphragm Contribution, %
Flat kraft	2.1
6% Extensible	3.7
9% Extensible	4.3
12% Extensible	4.7

DISCUSSION OF RESULTS

The biaxial tensile energy absorption of 26 samples of 50-lb., unbleached kraft sack paper was calculated from tests performed on a pressure-type biaxial tester constructed for this investigation. A major objective of the study is to examine the relationship between biaxial and uniaxial energy absorption, the latter determined by the conventional tensile test. As a necessary preliminary, attention is given first to the behavior of the specimen in the biaxial tensile test.

DISTENTION OF SPECIMEN

The distention at rupture of the sack paper samples is given in Table III. Each entry is the average of six specimens.

In Table III $\underline{w}_o$ is the distention at the center of the specimen; $\underline{w}_x$ is the distention at a point 2.8 in. from the center on the machine-direction meridian of the specimen; $\underline{w}_y$ is the distention on the cross-direction meridian 2.8 in. from the center. The average center distention was 0.535 in. for flat kraft and 1.005 in. for extensible kraft; in general, the distention increases with extensibility of the paper, as would be anticipated.

The right-hand-most column of Table III shows the ratio of $\underline{w}_x$ to $\underline{w}_y$. It may be seen that the ratio is very near unity. No deviation between $\underline{w}_x$ and $\underline{w}_y$ is in excess of 3% of the average off-center distention; stated another way, the maximum deviation between $\underline{w}_x$ and $\underline{w}_y$ is 1.7% of the center distention. This indicates that the distention surface is approximately a surface of revolution (that is, symmetrical about the center point), contrary to what might be expected of an anisotropic material. It may be noted, however, that the ratio is generally slightly less than unity for flat krafts and slightly greater than unity for extensible krafts. This seems to be in keeping with the presumed effect of anisotropy,

TABLE III

DISTENTION OF BIAXIAL TEST SPECIMENS

Sample	Type of Paper	Distention at Failure, in. Center, w_o	M.D., w_x	C.D., w_y	w_x/w_o	w_y/w_o	w_x/w_y
AA	Flat kraft	0.591	0.339	0.344	0.574	0.582	0.985
BB	" "	.541	.309	.312	.571	.577	.990
CC	" "	.582	.328	.330	.564	.567	.994
DD	" "	.530	.308	.299	.581	.564	1.030
EE	" "	.516	.296	.299	.574	.579	.990
FF	" "	.509	.291	.298	.572	.585	.977
GG	" "	.526	.303	.305	.576	.580	.993
HH	" "	.475	.270	.275	.568	.579	.982
II	" "	.543	.306	.313	.564	.576	.978
JJ	" "	.538	.308	.309	.572	.574	.997
KK	" "	.546	.307	.310	.562	.568	.990
LL	" "	.528	.301	.301	.570	.570	1.000
	Average:	0.535	0.306	0.308	0.571	0.575	0.992
MM	6% Extensible	0.976	0.587	0.587	0.601	0.601	1.000
NN	9% "	.968	.572	.571	.591	.590	1.002
OO	12% "	1.013	.612	.600	.604	.592	1.020
PP	6% "	.988	.581	.594	.588	.601	.978
QQ	9% "	1.063	.633	.637	.595	.599	.994
RR	12% "	1.113	.662	.649	.595	.583	1.020
SS	6% "	.912	.540	.543	.592	.595	.994
TT	9% "	.983	.581	.583	.591	.593	.997
UU	12% "	1.004	.594	.587	.592	.585	1.012
VV	9% "	1.054	.630	.628	.598	.596	1.003
WW	9% "	.997	.589	.594	.591	.596	.992
XX	9% "	.926	.534	.529	.577	.571	1.009
YY	9% "	.996	.614	.614	.616	.616	1.000
ZZ	12% "	1.074	.664	.648	.618	.603	1.025
	Average:	1.005	0.600	0.597	0.596	0.594	1.003
	Composite average:	0.788	0.464	0.464	0.584	0.585	0.998

that is, somewhat lower distention on the meridian having the lower stretch. For example, M.D. stretch is the lesser in flat kraft and accordingly the distention on the M.D. meridian is slightly lower; the converse generally holds for extensible kraft. The effect is evidently small, however, and the assumption of a symmetrical distention surface is quite appropriate for practical purposes, as has been assumed in the theoretical considerations of this investigation. One implication of these results is that the machine- and cross-direction strains are equal at the center of the specimen.

According to the Hencky-Stevens theory, the off-center distention (at $\underline{r}$ = 2.8 in.) should be 54.2% of the center distention, that is, $\underline{w}_x/\underline{w}_o = \underline{w}_y/\underline{w}_o = 0.542$ [see Appendix B]. The corresponding ratio for a spherical surface [see Appendix C] depends on $\underline{w}_o/\underline{a}$, where $\underline{a}$ is orifice radius. Table IV shows the relative values of off-center distention assuming a spherical surface for the samples of this study, as well as the Hencky-Stevens and the observed ratios. This comparison shows that the observed distention surface has slightly greater curvature than either the Hencky-Stevens or the spherical surface, as indicated by the higher ratio of $\underline{w}/\underline{w}_o$. Stated another way, for a given center distention, the observed surface bulges more in the region between center and perimeter than do the theoretical surfaces.

The effect of this difference between observed and theoretical distention surfaces on the calculated biaxial energy absorption at the center of the specimen is not entirely clear. Very likely the curvature at the center is overestimated by the Hencky-Stevens theory since it underestimates the true curvature at $\underline{r}$ = 2.8 inches. Reference to Equation (21), Appendix B reveals that the calculated biaxial energy absorption at the center, based on Hencky-Stevens theory, therefore underestimates the actual energy absorption. Presumably, the error is small, how-

TABLE IV

COMPARISON OF OBSERVED AND THEORETICAL DISTENTION SURFACES

$\frac{\text{Average Off-Center Distention}}{\text{Average Center Distention}}, \frac{w}{w_o} \; r = 2.8$

	Flat Kraft	Extensible Kraft	Combined
Observed	0.573	0.595	0.584
Hencky-Stevens[d]	0.542	0.542	0.542
% Diff.[d]	- 5.4	- 8.9	- 7.2
Spherical[d]	0.516[a]	0.526[b]	0.521[c]
% Diff.[d]	- 9.9	-11.6	-10.8

[a] $w_o/a = 0.134$

[b] $w_o/a = 0.251$

[c] $w_o/a = 0.197$

[d] Based on observed.

ever, because all distention surfaces under consideration are virtually coincident at the center (as well as near the periphery) of the specimen.

It may be questioned, of course, whether the apparent difference between theoretical and observed distention surfaces is due to measurement error. One source of error in the measured off-center distentions ($\underline{w}_{\underline{x}}$ and $\underline{w}_{\underline{y}}$) is associated with the spherical tip of the deflectometer probe. Ideally the probe should be pointed; however, a spherical tip was used to remove the possibility of piercing the paper. An effect of the spherical tip is to move the point of contact with the specimen slightly toward the center as the specimen bulges. This causes a small overstatement of the distentions $\underline{w}_{\underline{x}}$ or $\underline{w}_{\underline{y}}$ at $\underline{r}$ = 2.8 in. An analysis of this error shows that, on the average, $\underline{w}_{\underline{x}}$ or $\underline{w}_{\underline{y}}$ is in error by 0.0022 in. at the instant of specimen failure. This error is less than 0.3% of the center distention and is regarded as negligible. It is also a negligible portion of the apparent difference between the theoretical and observed distention surfaces.

It seems unlikely that a systematic calibration error in the deflectometers causes the difference between theory and observation, for the following reason. Comparison of surfaces involves the ratio of off-center to center distention. If all distention measurements were systematically in error in one direction (due, for example, to calibration error of the deflectometers or the oscilloscopes) the ratio $\underline{w}/\underline{w}_{\underline{o}}$ should be but little affected. It seems likely, therefore, that the difference between observed and theoretical distention surfaces is real and not a result of measurement error.

The Hencky-Stevens surface is a better approximation to the observed surface than is the spherical surface. However, the Hencky-Stevens surface underestimates the observed bulge of the specimen by about 7% at the point of measurement used in this study and, accordingly, the calculated energy absorption (based

on the Hencky-Stevens surface) can be expected to slightly underestimate the true energy absorption of the specimen.

NATURE OF FAILURE

Three general types of specimen failure patterns were experienced in the test, as illustrated in Fig. 11. They are: (a) line failure, (b) branched line failure, and (c) crescent. Line failures ran in one of the principal directions of the sheet, frequently but not always through the center of the specimen. A line failure which would be caused by tension stresses parallel to the machine direction is designated as an "M.D. line failure," and analogously for C.D. tension failures.

Branched line failures were oriented primarily in one principal direction and are further characterized by the direction of stress (M.D. or C.D.) which might reasonably have caused them. Crescent-shaped failures are designated according to the direction of stress which would cause rupture at the center (as contrasted with the ends) of the crescent. The axis of "symmetry" of the crescent generally coincided with a principal axis. Interpretation of these failures involves the assumption that failure originated at the center of the crescent.

A tally of the several types of failure observed in specimens of this study is given in Table V. It may be seen that all of the flat kraft failures are associated with machine-direction tension, as would be anticipated since the machine direction is the direction of lower stretch. Allowing for the uncertainty of the crescent-type failure stress, it remains that 97% of the specimens definitely appeared to fail in machine-direction tension.

With the extensible papers all but three of the 84 specimens failed in a direction associated with cross-direction tension. This is in keeping with the lower stretch in the cross direction of extensible papers. Allowing for uncertainty

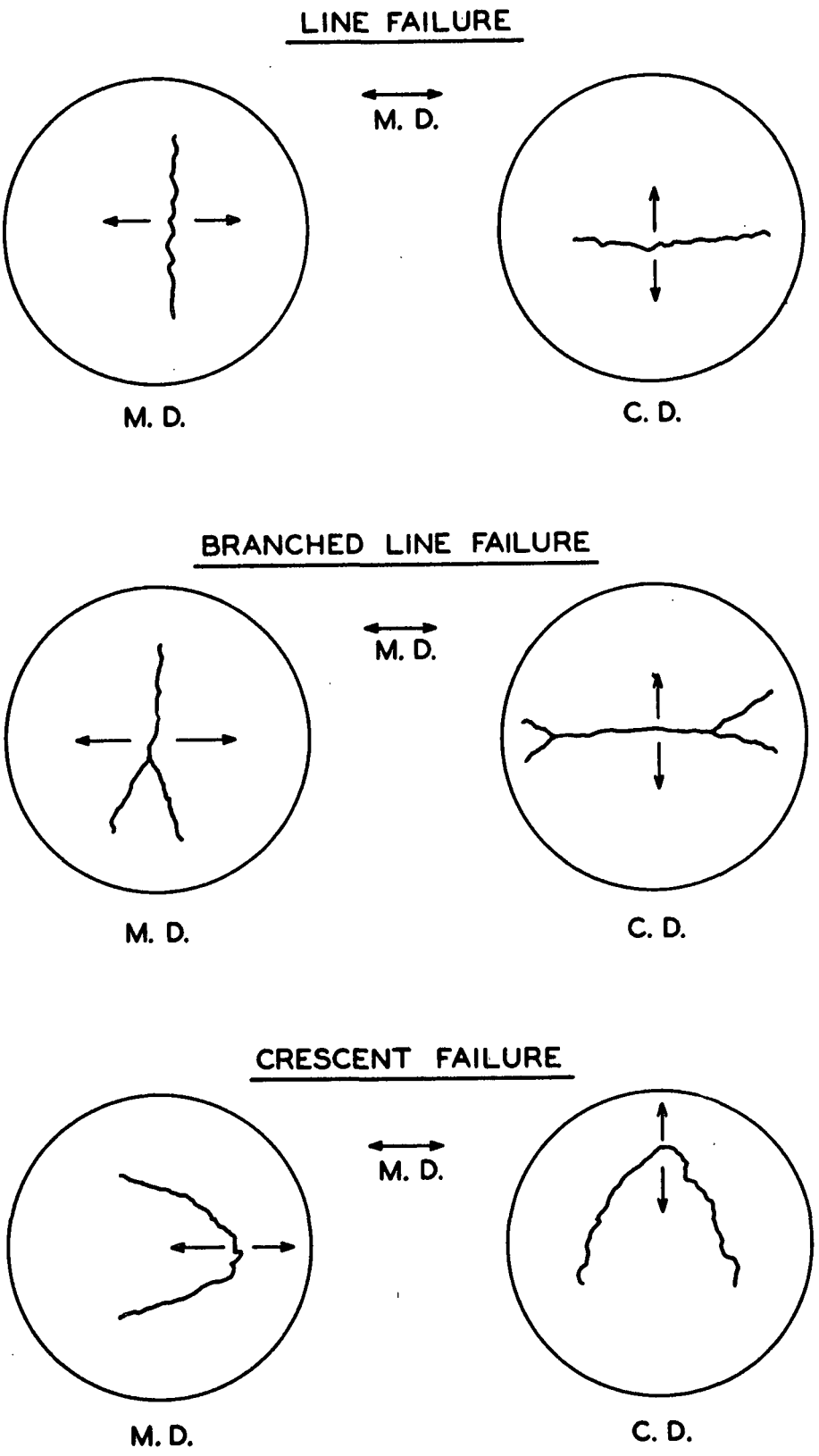

Figure 11. Nature of Failure in Biaxial Test Specimens

TABLE V

NATURE OF FAILURE

Sample	Type of Paper	Line Failure M.D. Tension	Line Failure C.D. Tension	Branch Failure M.D. Tension	Branch Failure C.D. Tension	Crescent Failure M.D. Tension[a]	Crescent Failure C.D. Tension[a]	Total
AA	Flat kraft	3		3				6
BB	" "	4		2				6
CC	" "	5		1				6
DD	" "			6				6
EE	" "	2		4				6
FF	" "	2		4				6
GG	" "	2		4				6
HH	" "			6				6
II	" "	2		4				6
JJ	" "			6				6
KK	" "	1		4		1		6
LL	" "			5		1		6
	Total:	21		49		2		72
	Percent:	29.2		68.0		2.8		100.0
MM	6% Extensible		1		2		3	6
NN	9% "		5				1	6
OO	12% "		6					6
PP	6% "		1		1	2	2	6
QQ	9% "		4		2			6
RR	12% "		6					6
SS	6% "		1		1		4	6
TT	9% "		3			1	2	6
UU	12% "		6					6
VV	9% "		6					6
WW	9% "		6					6
XX	9% "		6					6
YY	9% "		4				2	6
ZZ	12% "		6					6
	Total:		61		6	3	14	84
	Percent:		72.6		7.1	3.6	16.7	100.0

[a] Assumes failure initiated at center of crescent,

of the crescent-type failure, 80% of the extensible specimens definitely appeared to fail in cross-direction tension.

It seems clear, therefore, that failure of the biaxial test specimen is generally caused by exceeding the lesser of the two principal stretches of the sheet. This is generally believed to be true in the Mullen bursting strength test also (16).

Inasmuch as the biaxial specimen evidently fails in the direction of lesser stretch, it is of interest to estimate the failure strain at the center of the biaxial specimen and compare it with the lesser of the two principal uniaxial stretches evaluated by means of an Instron testing machine. Biaxial stretch is estimated by means of Equation (3) in THEORETICAL CONSIDERATIONS which involves the average Poisson ratio $\bar{\mu}$ (average, by assumption), center distention w_o and orifice radius a. Table VI lists the Poisson ratios, their average, the calculated biaxial stretch at the center, and the lesser Instron stretch.

It may be seen that the biaxial stretch was generally smaller than the M.D. uniaxial stretch of the flat kraft samples – by 9%, on the average. On the other hand, the biaxial stretch generally exceeded the C.D. Instron stretch of the extensible papers – by 15%, on the average. The systematic nature of these differences may stem in part from the uncertainty as to the proper combination of Poisson ratios for an anisotropic material such as paper when applying Equation (3).

BIAXIAL ENERGY ABSORPTION

The biaxial energy absorption $\Delta\bar{V}$ (in.-lb./in.^{2}) of each specimen of sack paper was calculated by means of Equation (2) in THEORETICAL CONSIDERATIONS. This is the energy absorption at the center of the specimen (the most highly stressed region). The energy absorption is estimated from the measured pressure and distention

TABLE VI

POISSON RATIOS AND COMPARISON OF BIAXIAL AND UNIAXIAL STRETCH

Sample	Type of Paper	Poisson Ratio			Stretch, %		
		Machine-Direction[a]	Cross-Direction[b]	Average	Biaxial[c]	Minimum Uniaxial	Diff., %[d]
AA	Flat kraft	0.294	0.236	0.265	1.61	1.8	- 11
BB	" "	.316	.211	.264	1.34	1.6	- 16
CC	" "	.212	.198	.205	1.69	1.4	+ 21
DD	" "	.412	.137	.274	1.26	1.5	- 16
EE	" "	.256	.183	.220	1.30	1.4	- 7
FF	" "	.314	.207	.260	1.19	1.4	- 15
GG	" "	.345	.214	.280	1.25	1.3	- 4
HH	" "	.270	.186	.228	1.09	1.4	- 22
II	" "	.255	.186	.220	1.44	1.6	- 10
JJ	" "	.306	.178	.242	1.36	1.6	- 15
KK	" "	.321	.227	.274	1.34	1.4	- 4
LL	" "	.331	.156	.244	1.32	1.5	- 12
	Average:	0.303	0.193	0.248	1.35	1.5	- 9
MM	6% Extensible	0.164	0.164	0.164	4.98	5.0	0
NN	9% "	.154	.194	.174	4.84	4.4	+ 10
OO	12% "	.131	.216	.174	5.29	4.4	+ 20
PP	6% "	.185	.172	.178	5.01	4.9	+ 1
QQ	9% "	.184	.173	.178	5.82	5.2	+ 12
RR	12% "	.119	.142	.130	6.72	5.4	+ 24
SS	6% "	.175	.119	.147	4.44	4.3	+ 3
TT	9% "	.187	.158	.172	5.01	4.6	+ 11
UU	12% "	.150	.134	.142	5.41	5.1	+ 6
VV	9% "	.160	.167	.164	5.83	4.8	+ 21
WW	9% "	.188	.129	.158	5.22	4.4	+ 19
XX	9% "	.151	.190	.170	4.47	3.6	+ 24
YY	9% "	.174	.155	.164	5.18	4.8	+ 8
ZZ	12% "	.150	.215	.182	5.88	4.0	+ 47
	Average:	0.161	0.167	0.164	5.29	4.6	+ 15
	Composite average:	0.236	0.178	0.203	3.47	3.2	+ 4

[a] Tension in machine direction; contraction in cross direction.

[b] Tension in cross direction; contraction in machine direction.

[c] Calculated from Equation (3).

[d] Based on uniaxial.

tion of the specimen, based on the Hencky-Stevens distention surface, and using the average of the M.D. and C.D. Poisson ratios. The average for the six specimens from each sample of paper is shown in Table VII in the column headed "Observed Biaxial Energy Absorption, $\Delta\overline{V}$".

A primary motive for studying biaxial energy absorption is to find its relationship to the conventional uniaxial energy absorptions in the two principal directions. While biaxial energy absorption (at an appropriate strain ratio) is intuitively pertinent to sack performance, uniaxial energy absorptions have greater utility from the standpoints of (a) availability of test equipment and (b) interpretation in terms of papermaking variables. The Instron tensile energy absorption (T.E.A.) in the principal directions is also shown in Table VII. These are for the outer-ply samples and are taken from Reference (4). The composite energy absorption shown in Table VII is the sum of the uniaxial energy absorptions.

It may be seen that the observed biaxial energy absorption at the center of the specimen is greater than the lesser uniaxial T.E.A. in all cases — that is, greater than M.D. T.E.A. of flat kraft and greater than C.D. T.E.A. of extensible kraft. This is to be expected; although the biaxial specimen fails at approximately the lesser of M.D. and C.D. stretch, there is a contribution to biaxial energy absorption from the stress and strain in the other principal direction.

On the other hand, with one exception, the biaxial energy absorption is always less than the sum (composite) of the uniaxial energy absorptions. This also is to be expected because the specimen does not reach the full stretch in the direction of higher uniaxial stretch.

Thus, the biaxial energy absorption lies intermediate to the minimum uniaxial energy absorption and the sum of the uniaxial energy absorptions. These relationships are displayed as correlation graphs in Fig. 12 and 13.

TABLE VII

COMPARISON OF BIAXIAL AND UNIAXIAL ENERGY ABSORPTION

Sample	Type of Paper	Instron Energy Absorption, in.-lb./in.^{2} M.D.	C.D.	Composite[a]	Estimated Biaxial,[b] $\underline{U}$	Observed Biaxial Energy Absorption,[c] $\Delta\overline{V}$, in.-lb./in.^{2}	Difference, $(\underline{U}-\Delta\overline{V})/\Delta\overline{V}$, %
AA	Flat kraft	0.422	0.496	0.918	0.629	0.741	- 15.1
BB	" "	.362	.444	.806	.517	.598	- 13.5
CC	" "	.292	.530	.822	.396	.693	- 42.9
DD	" "	.386	.418	.804	.532	.612	- 13.1
EE	" "	.332	.353	.685	.457	.576	- 20.7
FF	" "	.234	.344	.578	.360	.462	- 22.1
GG	" "	.290	.545	.835	.422	.595	- 29.0
HH	" "	.266	.420	.686	.415	.479	- 13.4
II	" "	.328	.414	.742	.523	.656	- 20.3
JJ	" "	.378	.525	.903	.544	.621	- 12.4
KK	" "	.262	.523	.785	.408	.584	- 30.1
LL	" "	.322	.527	.849	.489	.600	- 18.5
	Average:	0.323	0.462	0.784	0.474	0.601	- 20.9
MM	6% Extensible	0.943	0.760	1.703	1.452	1.716	- 15.4
NN	9% "	1.169	.641	1.810	1.103	1.497	- 26.3
OO	12% "	1.470	.680	2.150	1.044	1.537	- 32.1
PP	6% "	.980	.584	1.564	1.259	1.505	- 16.3
QQ	9% "	1.370	.602	1.972	1.199	1.648	- 27.2
RR	12% "	1.558	.648	2.206	1.146	1.655	- 30.8
SS	6% "	.991	.467	1.458	1.031	1.271	- 18.9
TT	9% "	1.239	.548	1.687	1.038	1.418	- 26.8
UU	12% "	1.490	.620	2.110	1.072	1.353	- 20.8
VV	9% "	1.352	.589	1.941	1.098	1.732	- 36.6
WW	9% "	.990	.508	1.498	.945	1.247	- 24.2
XX	9% "	1.293	.416	1.709	.717	1.045	- 31.4
YY	9% "	1.209	.540	1.749	1.030	1.457	- 29.3
ZZ	12% "	1.348	.502	1.850	.856	1.585	- 46.0
	Average:	1.243	0.579	1.815	1.071	1.476	- 27.3
	Composite average:	0.818	0.525	1.339	0.795	1.072	- 24.4

[a] Sum of M.D. and C.D. T.E.A.

[b] Sum of M.D. and C.D. energy absorption at the lesser of M.D. and C.D. stretch, $\underline{U} = \underline{U}_1 + \underline{U}_2$.

[c] Calculated by means of Equation (2).

[d] Based on "observed biaxial",

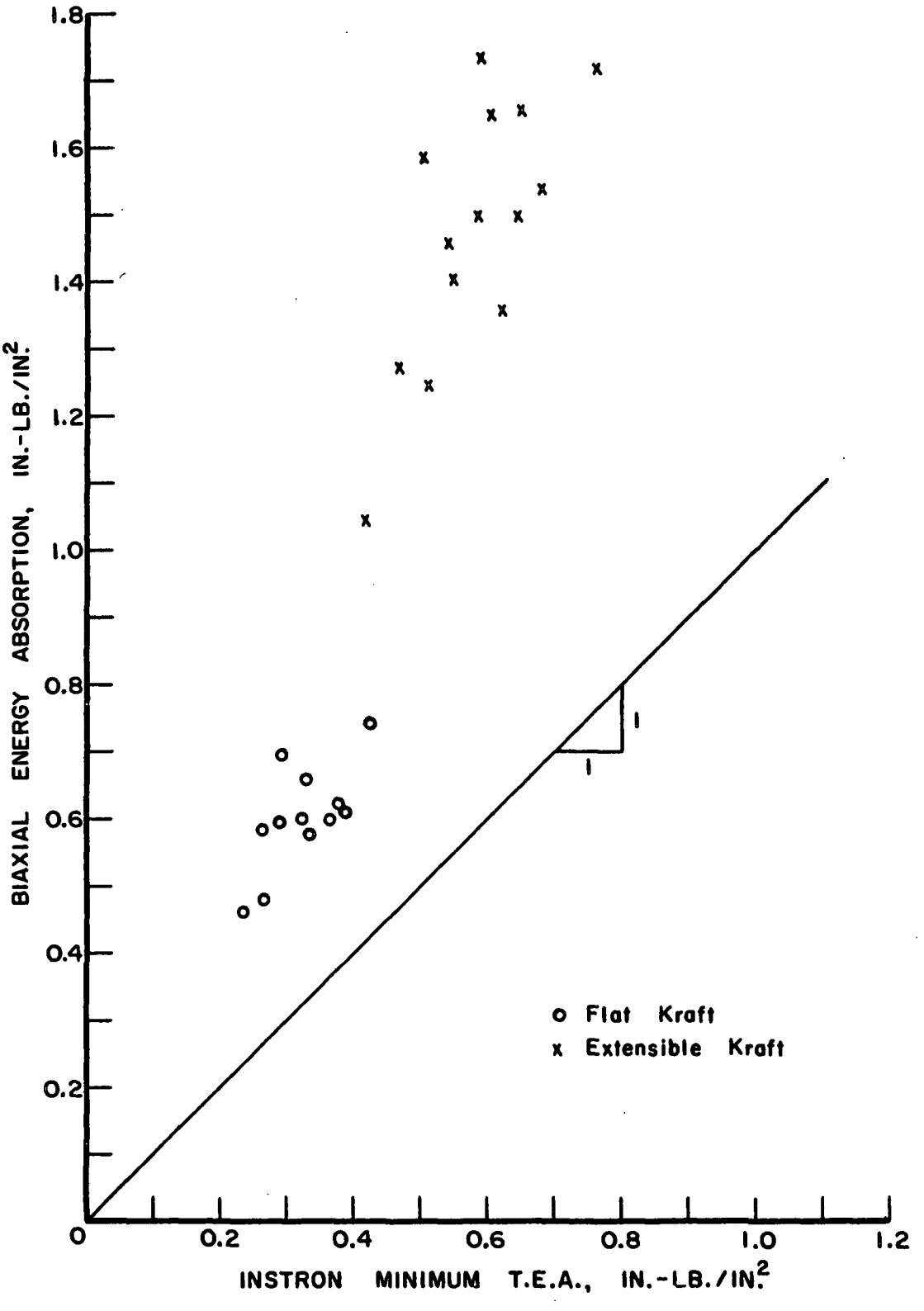

Figure 12. Relationship Between Biaxial Energy Absorption and Instron Minimum T.E.A.

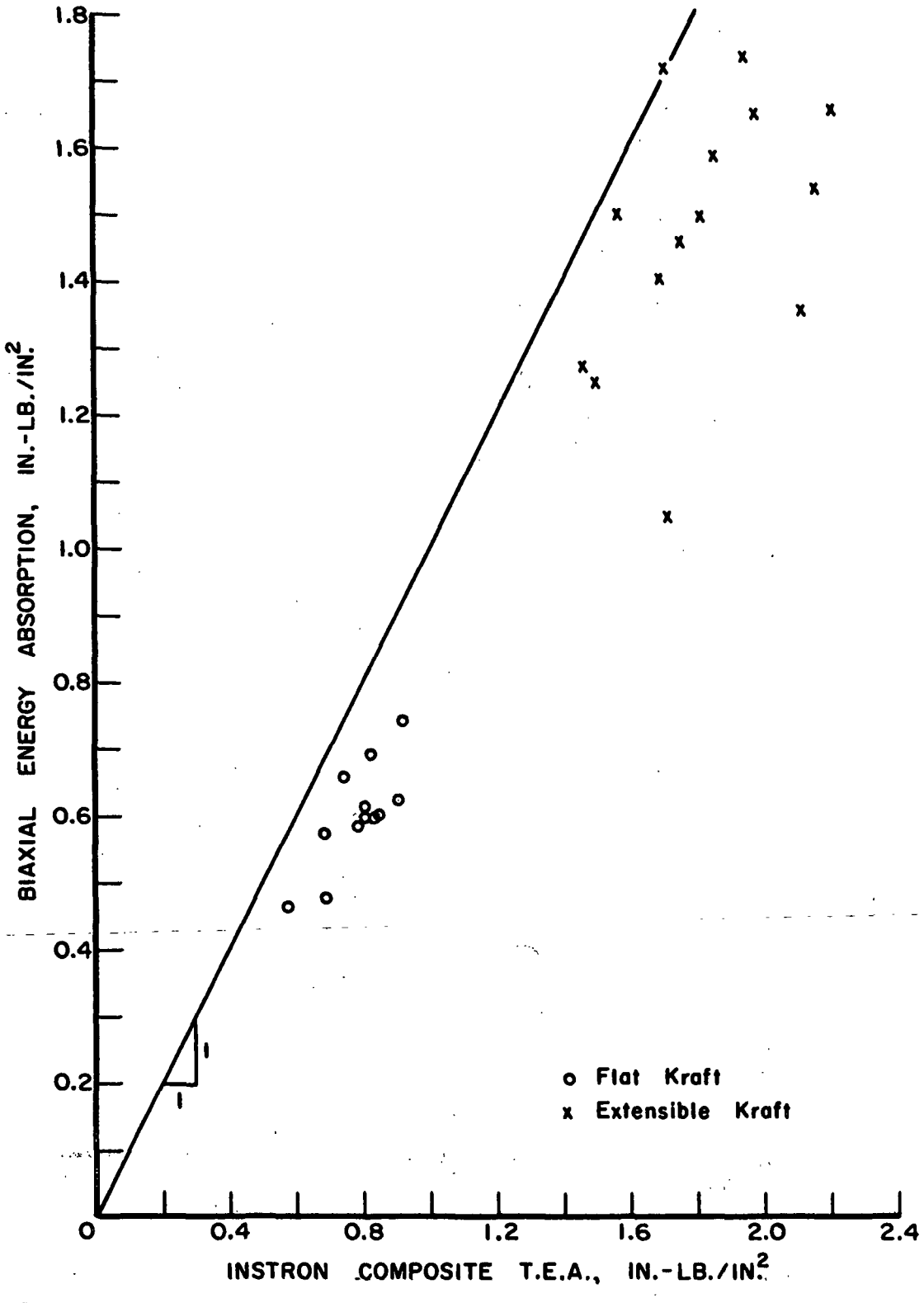

Figure 13. Relationship Between Biaxial Energy Absorption and Instron Composite T.E.A.

As mentioned above, the reason that composite T.E.A. overestimates biaxial energy absorption at the center of the specimen is that a portion of the T.E.A. in the direction of higher stretch is not realized in the biaxial test. It might be anticipated, therefore, that only the portion of the high-stretch-direction T.E.A. up to the stretch of the lesser-stretch-direction should be included. This is illustrated in Fig. 14. In the case of flat kraft, for example, machine-direction stretch governs failure and all of the M.D. T.E.A. [$\underline{U}_1$ in Fig. 14 (a)] should be effective; in the cross direction, however, only the portion $\underline{U}_2$ of the C.D. T.E.A. should be effective (where $\underline{U}_2$ terminates at a strain equal to the machine-direction stretch). Thus, an estimate of biaxial energy absorption, based on the uniaxial stress-strain curves, is

$$\underline{U} = U_1 + U_2 \qquad (7).$$

This is termed "Estimated Biaxial, $\underline{U}$" in Table VII. The contribution $\underline{U}_2$ was obtained by planimeter on the Instron load-elongation curves.

An analogous situation holds for extensible papers, as illustrated in Fig. 14 (b), where the roles of M.D. and C.D. are reversed from those of flat kraft.

As may be seen in Table VII or Fig. 15, the estimate $\underline{U}$ of biaxial energy absorption, based on uniaxial tension curves, consistently underestimates the observed biaxial energy absorption. On the average, the estimate is 21% low for flat kraft, 27% low for extensible kraft, and 24% low for all samples studied. There is a theoretical reason why this happens. As demonstrated in Appendix D, the biaxial energy absorption should exceed $\underline{U}_1 + \underline{U}_2$ because of the Poisson effect. This may be explained as follows: In either uniaxial or biaxial tension the energy contribution from, say, the machine direction ($\underline{x}$-direction) of the paper is $\int \sigma_{\underline{x}} d\epsilon_{\underline{x}}$. However, in biaxial tension, contraction in the $\underline{x}$-direction due to $\sigma_{\underline{y}}$ requires that $\sigma_{\underline{x}}$ be

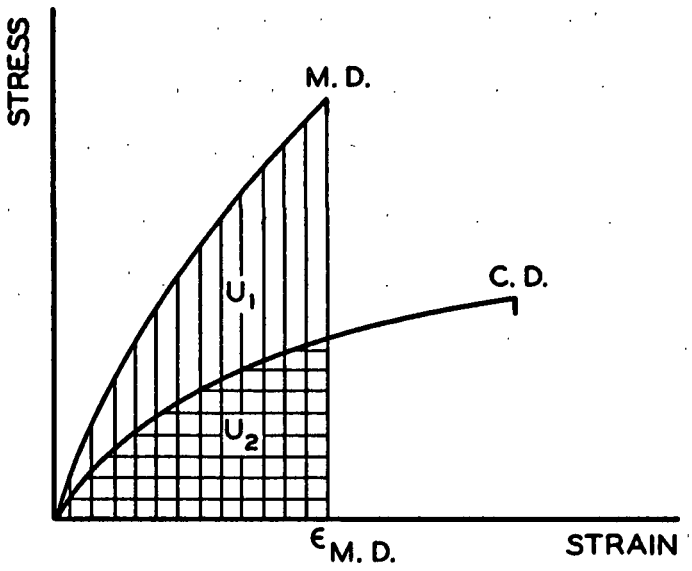

(a) FLAT KRAFT

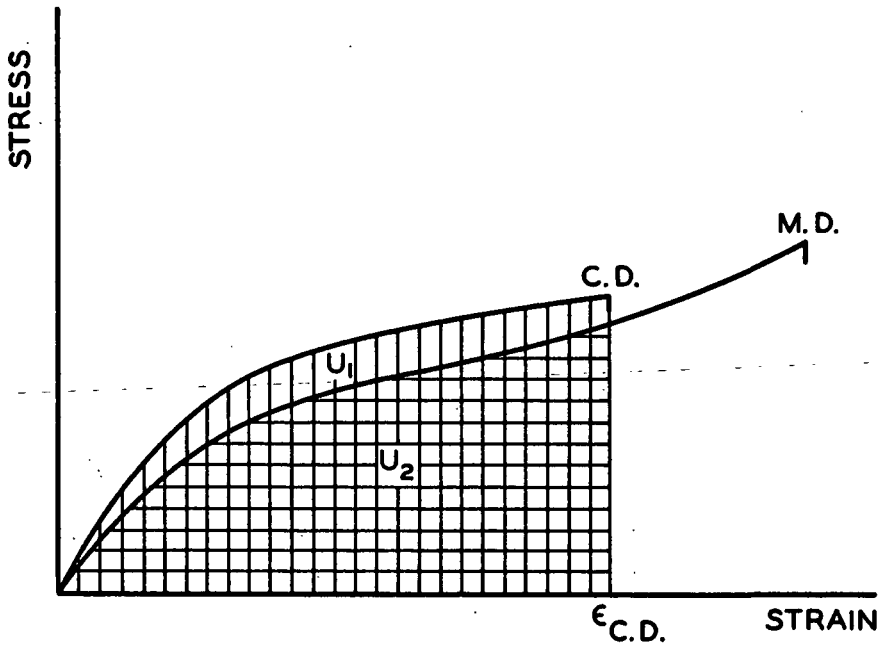

(b) EXTENSIBLE KRAFT

Figure 14. Method of Calculating Estimated Biaxial Energy Absorption $\underline{U}$ from Uniaxial Stress-Strain Curves ($\underline{U} = \underline{U}_1 + \underline{U}_2$)

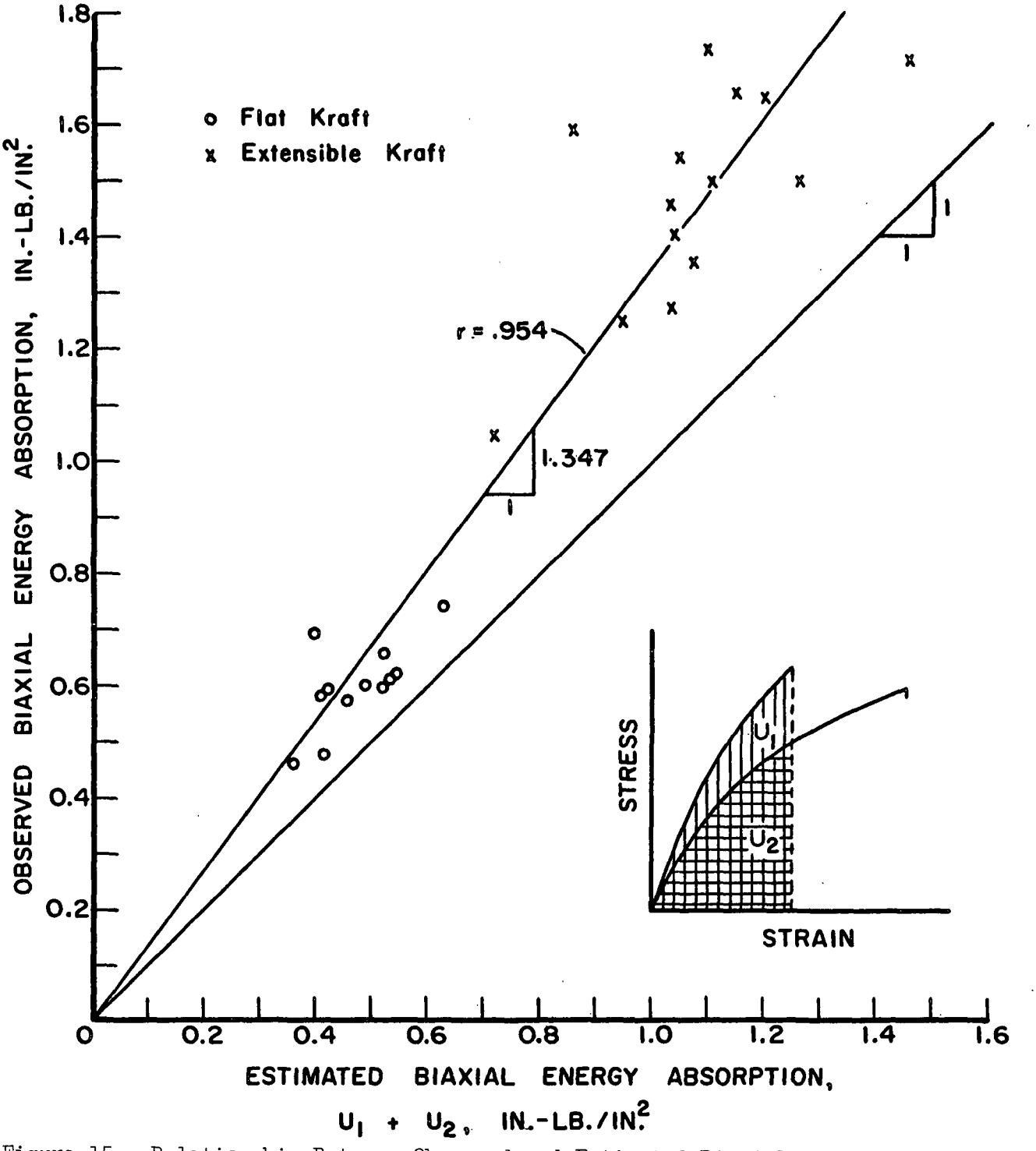

Figure 15. Relationship Between Observed and Estimated Biaxial Energy Absorption

larger than in the uniaxial case to give the same strain. Hence, $\int \sigma_{\underline{x}} d\epsilon_{\underline{x}}$ is greater in the biaxial case than in the uniaxial case. For the same reason the energy contribution in the y-direction is greater in biaxial tension than in uniaxial tension. Thus, the total biaxial energy absorption (both directions) is necessarily greater than $\underline{U}_1 + \underline{U}_2$, as borne out by the data. Estimation of the biaxial energy absorption from uniaxial tension data, accounting for the Poisson effect, is very difficult. It requires suitable mathematical approximations to the stress-strain (or load-elongation) curves in uniaxial tension and the functional relationship between the Poisson ratios and strain, as explained in Appendix D.

By way of summary, the several energy absorptions considered are ranked in the following order from smallest to largest:

1. Uniaxial T.E.A. in direction of minimum stretch
2. Estimated biaxial energy absorption, $\underline{U}$ (i.e., sum of M.D. and C.D. energy absorption at the lesser of M.D. and C.D. stretch)
3. Observed biaxial energy absorption, $\Delta\overline{\underline{V}}$
4. Composite (sum) of M.D. and C.D. T.E.A.

$\Delta\overline{\underline{V}}$ is greater than $\underline{U}$ because of the Poisson effect in biaxial tension. On the average, $\Delta\overline{\underline{V}} = 1.347\ \underline{U}$, as shown in Fig. 15; the average prediction error of this relationship is 10% for the samples of this study.

A reasonable next-phase in studying the relationship between biaxial and uniaxial energy absorption is to investigate strain ratios other than 1:1. As mentioned earlier, this may be accomplished with the biaxial tester by changing the orifice from circular to elliptical with various ratios of major and minor axes.

In this larger view, the data presented in this report locate three points on the energy "interaction" curve of each sample of sack paper. One way

of presenting the interaction curve is shown in Fig. 16. In this diagram the biaxial energy absorption $\Delta\bar{V}$ is expressed as a ratio of U, where U is obtained as illustrated in Fig. 14; however, ratios of strain other than 1:1 are under consideration and accordingly the components U_1 and U_2 terminate at different levels of strain in keeping with the strain ratio.

Strain ratio is plotted as the abscissa in the interaction diagram. The abscissa is not scaled in the conventional manner of constructing a graph. The vertical axis is centered at a strain ratio of 1.0. The right-hand region of the graph corresponds to $\epsilon_x > \epsilon_y$ and the strain ratio ϵ_y/ϵ_x increases from right to left in this region. It should be noted that the strain ratio of the x-direction uniaxial tensile test is $-\mu_{xy}$. The left-hand region of the diagram is $\epsilon_x < \epsilon_y$ and analogous considerations apply.

The three known points on this diagram are the two uniaxial T.E.A.'s, for which $\Delta\bar{V}/U = 1.0$, and the biaxial energy absorption at $\epsilon_x/\epsilon_y = \epsilon_y/\epsilon_x = 1.0$, for which $\Delta\bar{V}/U = 1.347$, on the average, as determined in this study. The biaxial energy absorptions at intermediate strain ratios lie on some unknown curve (shown dashed) which would be the object of the recommended future study.

Knowledge of the typical shape(s) of such interaction curves based on representative samples of paper would enable one to estimate the biaxial energy absorption for a given strain ratio from the uniaxial energy absorptions derivable from uniaxial tensile tests, as are conventionally performed with paper. Used in the inverse sense, it should be possible to find the strain ratio giving maximum biaxial energy absorption (this may be different from 1:1) and to some extent, thereby, the most favorable ratio of sack dimensions since these in part govern strain ratio. Moreover, implicit in the interaction diagram is the effect of shape of the uniaxial tensile load-elongation curves; it should be possible, therefore, to project the

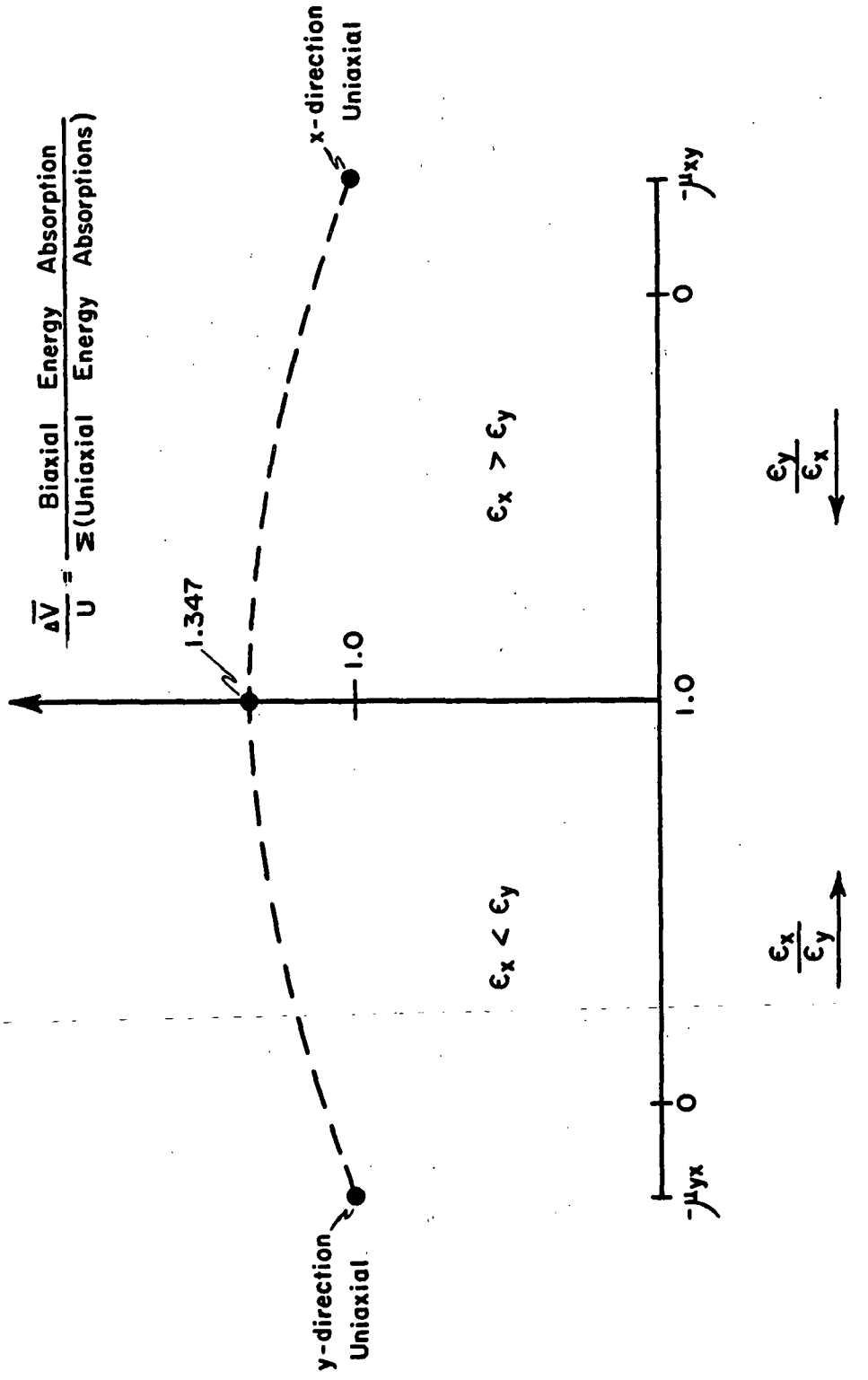

Figure 16. Hypothetical Interaction Curve for Biaxial Tensile Energy Absorption

effect of changes in uniaxial curve shape to potential biaxial energy absorption. All of these applications would be rendered much more feasible by the development of mathematical approximations to the load-elongation curves so that the estimates could be made by computation rather than by graphical integration.

CORRELATION BETWEEN BIAXIAL ENERGY ABSORPTION AND SACK PERFORMANCE

The above discussions have been concerned with the materials science aspects of this particular biaxial tension test – namely, the behavior of the specimen and the relationship between biaxial and uniaxial properties. It is, of course, appropriate to consider the degree of correlation between biaxial energy absorption, as evaluated by this method, and sack performance – progressive height face drop and butt drop. The performance values are given in Reference (4).

The relationships are summarized in Table VIII in terms of the correlation coefficient and the average (absolute) difference of prediction expressed as a percent. Correlation graphs are shown in Fig. 17 and 18. For purposes of comparison, Table VIII also shows the correlations for combined uniaxial T.E.A. (i.e., sum of M.D. and C.D. T.E.A.) and the multiple correlations with M.D. and C.D. T.E.A. [from Reference (5)]. All of the correlations summarized are significant at or beyond the 0.05 level.

It may be seen that, in progressive height face drop, the correlation with biaxial energy absorption is inferior to the T.E.A. correlations for the flat kraft samples. With the extensible samples and the combined data, all correlations are at about the same level. It should be kept in mind that biaxial energy absorption was evaluated on only the outer-ply sack paper, and this fact should favor the correlations involving T.E.A. because they reflect all three plies of the multiwall sacks.

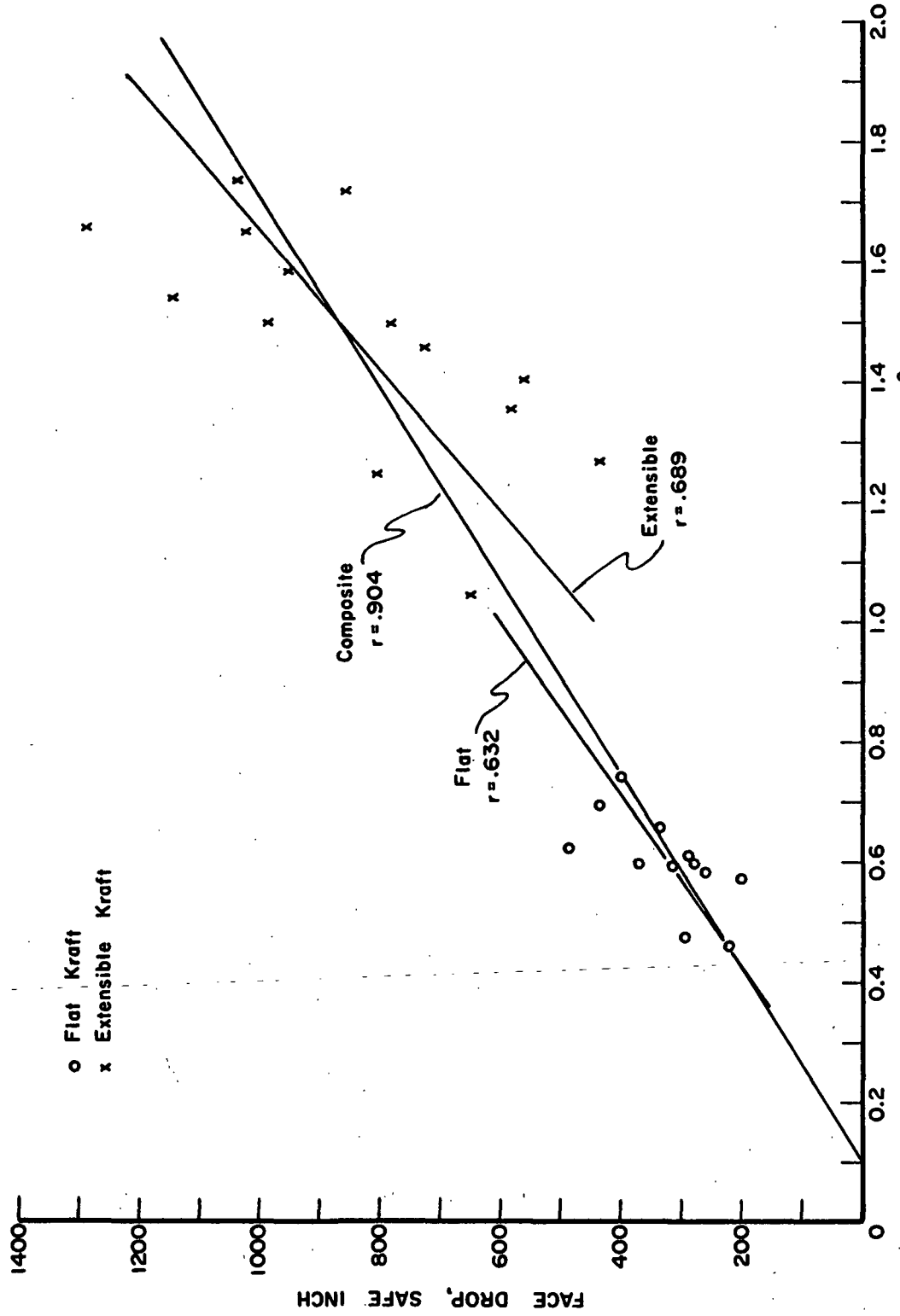

Figure 17. Relationship Between Biaxial Energy Absorption and Progressive Height Face Drop

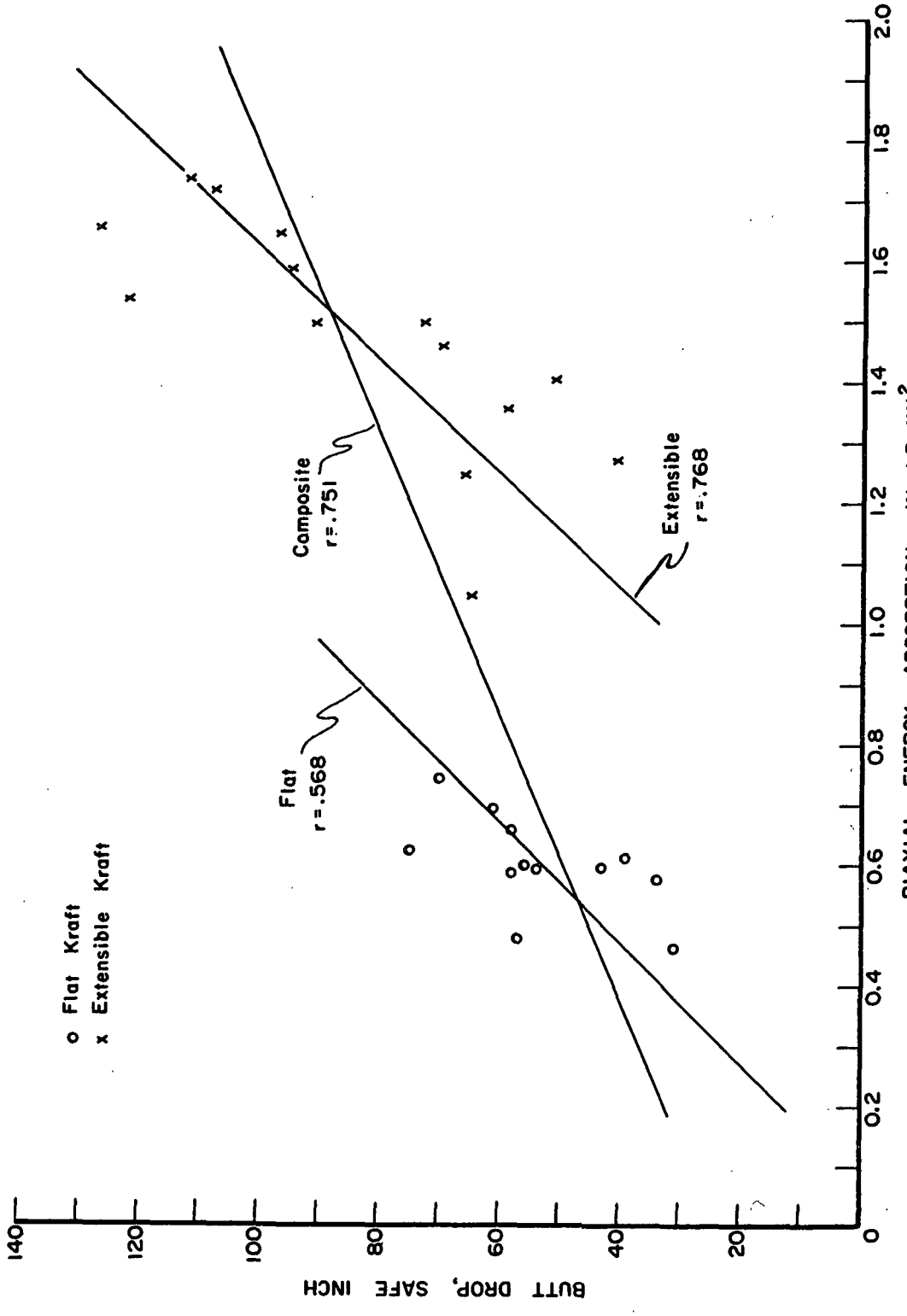

Figure 18. Relationship Between Biaxial Energy Absorption and Butt Drop

A somewhat similar comparison of correlations occurs with butt drop. It would be expected that neither biaxial energy absorption nor combined T.E.A. would be an efficient predictor of butt drop performance because this type of impact is found to depend primarily on cross-direction properties due to the nature of stress distribution in the sack walls.

Taken in their entirety, there is little to choose between the three types of energy absorption properties considered in Table VIII, on the basis of correlation with sack performance. The multiple regressions with T.E.A. are generally the best, however, no doubt because of the greater "flexibility" of the multiple regression technique. On conceptual grounds, all three measures of energy absorption suffer from two deficiencies as regards repeated sack impact. First, they are not repeated stress tests and do not therefore reflect the fatigue performance of sack paper. It has been visualized that the biaxial tester could be automated to repeatedly stress the specimen according to some arbitrary program of pressure, distention or energy absorption. Second, all energy absorptions considered are obtained at low test rates whereas sack impact occurs at high stress rates. This may not be a serious objection from the correlation standpoint because allied studies have shown reasonably good correlation between "static" and dynamic properties of sack paper (3, 18, 19).

Biaxial energy absorption, $\Delta\overline{V}$, as evaluated in this study, and combined T.E.A. also suffer from the fact that they take no account of the ratio of induced strain in the sack during impact. Use of combined T.E.A. implicitly assumes that both principal directions of the paper reach failure, which is contrary to observation and experiment. Biaxial energy absorption, $\Delta\overline{V}$, was evaluated in this study at essentially a 1:1 ratio of strain in the two principal directions, whereas experiment shows that the principal strains in sack impact are generally not equal (1, 2). The biaxial tester could be modified, however, to give other ratios of

TABLE VIII

CORRELATION BETWEEN ENERGY ABSORPTION AND SACK PERFORMANCE

Type of Paper	Biaxial Energy, $\bar{V}$		Combined T.E.A.		Multiple Correlation with M.D. and C.D. T.E.A.	
	Correlation Coefficient	Average Prediction, Diff., %	Correlation Coefficient	Average Prediction, Diff., %	Correlation Coefficient	Average Prediction, Diff., %
Progressive Height Face Drop						
Flat	0.63	16.0	0.83	12.3	0.84	12.1
Extensible	0.69	19.7	0.63	21.6	0.73	17.9
Composite	0.90	17.5	0.89[a]	18.4[a]	0.92[b]	19.1[b]
Butt Drop						
Flat	0.57	18.2	0.85	11.2	0.86	10.5
Extensible	0.77	19.0	--	--	0.82	17.8
Composite	0.75	23.3	0.65[a]	25.6[a]	0.86[b]	16.8[b]

[a] Based on 26 samples of present study plus 20 additional samples of flat kraft.

[b] Reference (4).

strain by introducing an elliptical orifice, as discussed in THEORETICAL CONSIDERATIONS. The multiple correlations involving M.D. and C.D. T.E.A. account for strain ratio in an empirical way through the regression coefficients (multiplying constants).

BURSTING PRESSURE IN BIAXIAL TEST

Bursting pressure in the biaxial test is of secondary interest in this investigation. The pressures obtained for the sack paper samples are presented in Table IX, however, for the possible interest they may have in other contexts, such as comparison with the conventional Mullen bursting strength. The diaphragm contribution has been removed from the pressure data so that the reported values pertain to the pressure resisted solely by the paper in the case of the biaxial data.

It may be seen that the burst pressure of these samples ranged from about three to five p.s.i.g., with flat kraft nearer the lower end of the range and extensible kraft nearer the higher end, in general. Figure 19 shows the correlation between these burst pressures and the conventional Mullen bursting strength pressure. The latter are reported in Reference (4) and range from approximately 30 to 60 p.s.i.g.; they include the Mullen diaphragm contribution. On the basis of theory (12, 16), the pressure required to give a specified strain at the center of a circular membrane varies inversely as the radius of the membrane (i.e., inversely as the orifice radius of the upper clamp of the testing machine). Inasmuch as the orifice radii of the Model C Mullen tester and the biaxial tester are 0.60 and 4.0 in., respectively, it would be anticipated from theory that the Mullen bursting strength is $4.0/0.60 = 6.67$ times the biaxial test pressure. This relationship is shown as the straight line labeled "Theoretical" in Fig. 19.

It may be seen that the Mullen bursting strengths are substantially greater than would be expected from the theory – by 10 to 25 p.s.i.g. (relative to

TABLE IX

BURSTING PRESSURE IN BIAXIAL TEST

Sample	Type of Paper	Pressure at Failure, p.s.i.g. Observed[a]	Estimated[b]	Diff., %[c]
AA	Flat kraft	3.96	4.46	+ 12.6
BB	" "	3.50	3.89	+ 11.1
CC	" "	3.50	3.28	- 6.3
DD	" "	3.82	4.36	+ 14.1
EE	" "	3.42	3.87	+ 13.2
FF	" "	2.94	3.20	+ 8.8
GG	" "	3.76	3.92	+ 4.3
HH	" "	3.08	3.70	+ 20.1
II	" "	3.59	4.13	+ 15.0
JJ	" "	3.63	4.31	+ 18.7
KK	" "	3.42	3.53	+ 3.2
LL	" "	3.49	4.06	+ 16.3
	Average	3.51	3.89	+ 10.9
MM	6% Extensible	4.81	5.83	+ 21.2
NN	9% "	4.23	5.08	+ 20.1
OO	12% "	4.17	5.30	+ 27.1
PP	6% "	4.24	5.13	+ 21.0
QQ	9% "	4.31	5.31	+ 23.2
RR	12% "	3.74	4.94	+ 32.1
SS	6% "	3.67	4.86	+ 32.4
TT	9% "	3.79	4.93	+ 30.1
UU	12% "	3.39	5.00	+ 47.5
VV	9% "	4.39	5.41	+ 23.2
WW	9% "	3.39	4.20	+ 23.9
XX	9% "	3.11	4.34	+ 39.5
YY	9% "	4.00	4.80	+ 20.0
ZZ	12% "	4.10	4.04	- 1.5
	Average:	3.95	4.94	+ 25.7
	Composite average:	3.75	4.46	+ 18.9

[a] Corrected for diaphragm contribution.

[b] $\underline{p} = \frac{2\sqrt{6}}{\underline{a}} \sqrt{\underline{e}} \left(\frac{\underline{T}_x + \underline{T}_y}{2} \right)$, where $\underline{e}$ is the lesser uniaxial stretch.

[c] Based on observed.

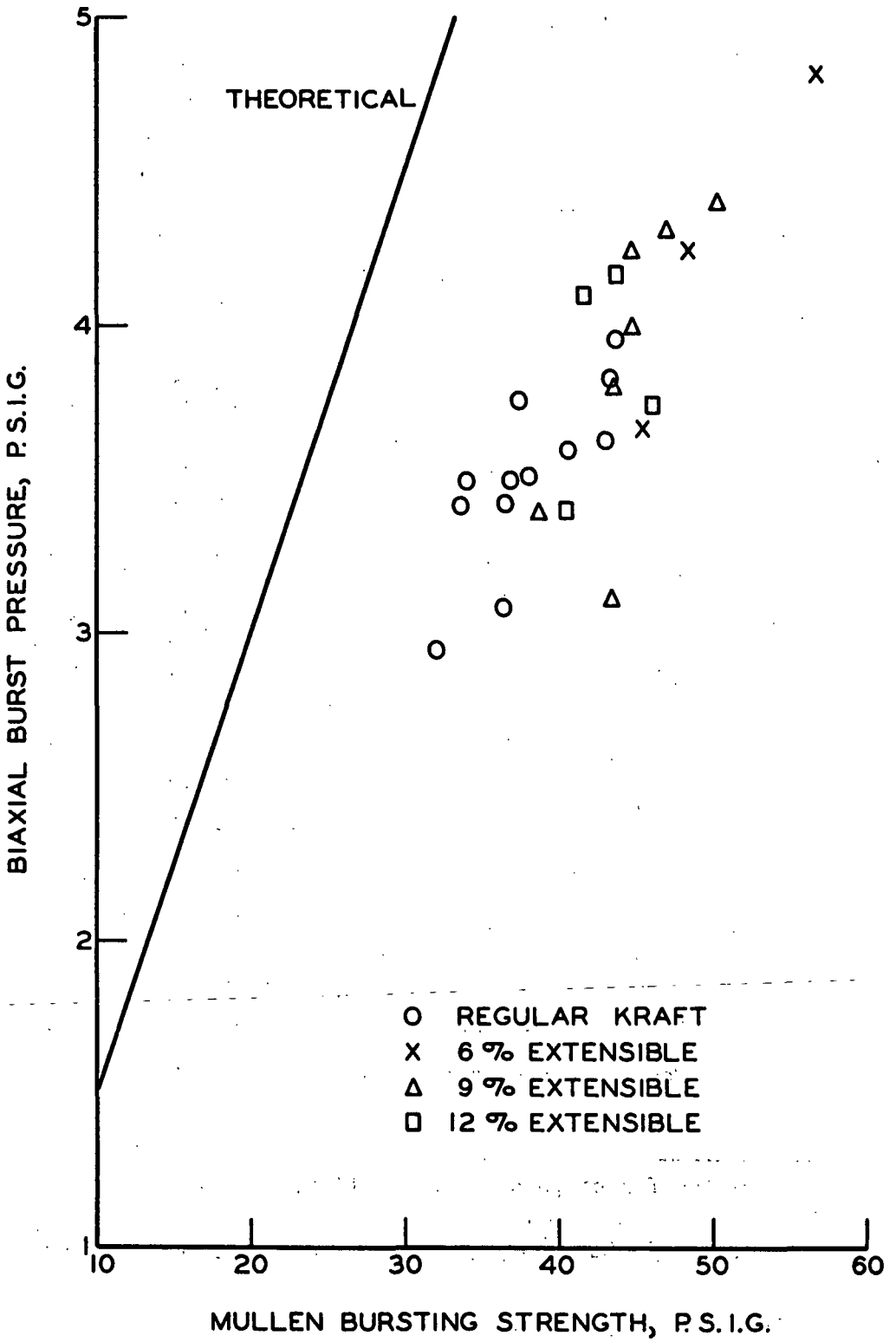

Figure 19. Relationship Between Burst Pressure from Biaxial Tester and Mullen Tester

the biaxial test pressures). The excess is attributable in part to the contribution of the rubber diaphragm in the Mullen tester. Another possible reason for the deviations is the smaller area of paper sampled in the Mullen test. In terms of, for example, the Peirce "weak link" theory, the smaller area tested in the Mullen test should lead to an increased apparent strength (20).

The observed bursting pressure in the biaxial test may be compared with a theoretical estimate originally devised in connection with the Mullen tester (16). The estimate, attributable to Van den Akker, is calculated from the following equation:

$$p = \frac{2\sqrt{6}}{a}\sqrt{e\left(\frac{T_x + T_y}{2}\right)} \qquad (8)$$

where p = burst pressure, lb./in.^{2}

a = orifice radius, in.

e = lesser stretch in the two principal directions of the sheet, in./in.

T_x = M.D. uniaxial tensile strength, lb./in.

T_y = C.D. uniaxial tensile strength, lb./in.

Equation (8) is derived on the assumption that the specimen bulges to a surface of revolution (symmetrical about the center point). Taking the average of the uniaxial tensile strengths in Equation (8) is an expedient; certainly the ultimate uniaxial tensile strengths in both principal directions are not reached simultaneously at failure because rupture occurs at the lesser principal stretch, as was pointed out in Reference (16). Tending to compensate for this overstatement of force levels is that the forces in biaxial tension should be higher than in the uniaxial test due to the Poisson effect.

Bursting pressure, estimated by means of Equation (8), and the difference from observed bursting pressure are shown in Table IX. It may be seen that Equation (8) generally overestimated the bursting pressure, by 10.9% for the flat kraft and by 25.7% for extensible kraft, on the average. The higher error with extensible paper possibly may arise because the "turn-up" of the M.D. load-elongation curve near ultimate causes T_x to severely overestimate the force contribution in this direction of the sheet.

EFFECT OF SHEET TWO-SIDEDNESS

In the main run of testing described above, the "felt"-side of the paper was uppermost in the tester. Thus, the "felt"-side was on the convex surface of the bulge during test and in this sense corresponds to the "felt"-side on the convex surface of the outer ply of a multiwall sack. A brief study was performed to determine the effect of "felt"-side up vs. wire-side up in the biaxial test. Five specimens were tested in each orientation for Samples AA, MM, and RR. The average pressures and center distentions are shown in Table X; for this comparison, pressure was not corrected for diaphragm contribution.

It may be seen that there is no consistent effect due to wire-side up vs. "felt"-side up on either pressure or distention. On the average, with the wire side up the bursting pressure was 4.4% higher and the center distention was 0.1% lower. An analysis of variance showed that neither effect was significant at the 0.05 level. It appears, therefore, that the two-sidedness of sack paper has no appreciable effect on the pressure and distention characteristics of the specimen in this biaxial tensile test.

It might be remarked that two-sidedness of the sheet does have a detectable effect on the Mullen bursting strength of paperboards. With 42-lb. linerboard, for

TABLE X

EFFECT OF SHEET TWO-SIDEDNESS ON RESULTS OF BIAXIAL TENSILE TEST

Sample	Type of Paper	Pressure, p.s.i.g.			Central Distention, w_o, in.		
		Wire Side Down	Wire Side Up	Diff., %[a]	Wire Side Down	Wire Side Up	Diff., %[a]
AA	Flat	4.00	4.16	+ 4.0	0.604	0.611	+ 1.2
MM	5% Extensible	5.22	4.94	- 5.4	1.050	0.989	- 5.8
RR	12% Extensible	3.91	4.48	+14.7	1.134	1.184	+ 4.4
			Av.	+ 4.4		Av.	- 0.1

[a] Based on wire-side down.

example, the bursting strength with the "felt"-side up generally runs about 10% higher than wire-side up. This effect is attributed to more extensive bonding (more fines and/or more highly refined stock) on the "felt"-side, leading to higher tensile strength on the "felt"-side of the sheet. The tensile stress imposed on the upper surface of the sheet in a bursting strength test is slightly higher than on the under surface because of a degree of flexure accompanying the overall membrane tension in the specimen. Thus, the higher tensile strength of the "felt"-side favors this surface uppermost in the bursting strength test. Flexure stresses can be expected to be of considerably less importance in the case of sack paper in the biaxial test; their magnitude varies inversely as the square of the orifice radius and directly as the thickness and thus the maximum bending stress in the biaxial sack paper specimen can be expected to be on the order of 1/100 that of the linerboard specimen in the Mullen bursting strength test. It is understandable, therefore, that no large effect was detected in this study.

It may be remarked that the statistical analysis revealed that the coefficients of variation of pressure and center distention were about 9-1/2% and 5-1/2%, on the average, for these three samples. These values reflect variability of (a) the sack paper and (b) the experimental measurements.

LITERATURE CITED

1. The Institute of Paper Chemistry. Investigation of the strains in a multiwall sack at the time of impact. Progress Report Nine, Project 2033, Sept. 8, 1959.

2. The Institute of Paper Chemistry. Development of a strain gage for sack paper. Part II. Progress Report Thirty-Eight, Project 2033, June 10, 1966.

3. The Institute of Paper Chemistry. A study of multiwall sack performance. Part I. Progress Report Twelve, Project 2033, Feb. 8, 1960.

4. The Institute of Paper Chemistry. A study of miltiwall sack performance. Part II. Progress Report Twenty-One, Project 2033, Oct. 1, 1962.

5. The Institute of Paper Chemistry. Relationship between sack drop and sack paper properties. Part III (Face Drop). Progress Report Thirty-Four. Part IV (Butt Drop). Progress Report Thirty-Seven, Project 2033, Jan. 17 and June 10, 1966.

6. Timoshenko, S. Strength of materials. Part II: Advanced theory and problems. p. 473. New York, D. van Nostrand Co., 1940.

7. Marin, J. Theory of strength for combined stresses and nonisotropic materials. J. Aero. Sci. 24, no. 4:265(1957).

8. Norris, C. B. Strength of orthotropic materials subjected to combined stresses. Madison, Wis. USDA Forest Service, Forest Products Laboratory, Report No. 1816, July, 1950.

9. The Institute of Paper Chemistry. A study of the biaxial stress-strain behavior of sack paper. Part I. Theoretical considerations and description of a static biaxial stress-strain tester. Progress Report Ten, Project 2033, Sept. 8, 1959.

10. The Institute of Paper Chemistry. A study of the biaxial stress-strain behavior of sack paper. Part II. Preliminary testing of sack paper employing a static biaxial stress-strain tester. Progress Report Eleven, Project 2033, Sept. 8, 1959.

11. The Institute of Paper Chemistry. Determination of the reinforcement afforded sack paper by an electrical resistance strain gage. Progress Report Eight, Project 2033, Sept. 8, 1959.

12. Hencky, H. Uber den spannungszustand in kreisrunder platten mit verschwinder bregungssteifigkeit. Z. Math. Phys. 63:311(1915).

13. Stevens, H. H. Behavior of circular membranes stretched above the elastic limit by air pressure. Proc. Exp. Stress Anal. II, no. 1:139-46(1944).

14. Roark, R. J. Formulas for stress and strain. p. 247. New York, McGraw-Hill Book Co., 1965.

15. Campbell, W. B. Relation of bursting to tensile tests. Forest Products Lab. Canada, Pulp Paper Lab., Quarterly Review no. 16:1-4(Oct.-Dec., 1933).

16. The Institute of Paper Chemistry. The meaning of the bursting strength test. Unpublished work.

17. Taylor, G. I. The scientific papers of. Edited by G. K. Batchelor. Vol. I. p. 496-502. Cambridge University Press, 1958.

18. The Institute of Paper Chemistry. Relationship between sack performance and the properties of sack paper. Part V. Progress Report Twenty-Five, Project 2033, Oct. 31, 1962.

19. The Institute of Paper Chemistry. Tension properties of sack paper at high rates of strain. Progress Report Thirty-Six, Project 2033, April 12, 1966.

20. Peirce, F. T. Tensile tests for cotton yarns. V. "The weakest link." J. Textile Inst. 17:T355(1926).

21. Thomson, W. T., unpublished notes, Univ. of Wisconsin, 1950.

22. Timoshenko, S., and Woinowsky-Krieger, S. Theory of plates and shells. p. 400. New York, McGraw-Hill Book Co., 1959.

23. Reference (6), p. 159.

24. March, H. W. Stress-strain relations in wood and plywood considered as orthotropic materials. Madison, Wis., USDA Forest Service, Forest Products Laboratory, Report No. R1503, Feb., 1944.

25. Timoshenko, S. Theory of elasticity. p. 8. New York, McGraw-Hill Book Co., 1934.

26. Reference (25), p. 136.

THE INSTITUTE OF PAPER CHEMISTRY

J. W. Gander
Research Associate

J. R. Wachuta
Research Assistant

R. C. McKee by wjw
R. C. McKee
Senior Research Associate, Container Section

APPENDIX A

SYMBOLS

a = radius of orifice (or semiaxis of ellipse), in.

A = area, $in.^2$

b = semiaxis of ellipse), in.

e = stretch, in./in.

E = Young's modulus of elasticity, $lb./in.^2$

M = area of reference rectangle on tracing, $in.^2$

p = pressure, $lb./in.^2$

P = calibration factor of pressure transducer, $lb./in.^2/cm.$

Q = calibration factor of deflectometer, in./cm.

r = radius nector in polar coordinates, in.

R = radius of curvature, $in.^{-1}$

S = area of reference rectangle on oscilloscope, $cm.^2$

t = thickness of specimen, in.

T = uniaxial tensile strength, lb./in.

U = uniaxial energy absorption, in.-lb./$in.^2$

V = work or energy, in.-lb.

$\overline{V}$ = average energy absorption per unit area of the entire specimen, in.-lb./$in.^2$

$\Delta\overline{V}$ = biaxial energy absorption per unit area in a small region at the center of the specimen, in.-lb./$in.^2$

V_o = biaxial elastic energy absorption per unit volume of an orthotropic material, in.-lb./$in.^3$

w = distention of specimen at an arbitrary point on specimen, in.

Θ = angle in polar coordinates, radian

φ = inclination of tangent line, radian

σ = stress, $lb./in.^2$

ϵ = unit strain, in./in.

μ = Poisson's ratio, dimensionless

$\bar{\mu}$ = composite of Poisson's ratios, dimensionless

Subscripts:

o = center of specimen

r = radial

s = secant

x = machine direction

y = cross-machine direction

max = maximum

θ = tangential

1 = direction of lesser uniaxial stretch

2 = direction of greater uniaxial stretch

m = minimum

APPENDIX B

ENERGY ABSORPTION RELATIONSHIPS FOR THE PRESSURE-TYPE BIAXIAL TESTER

The following two types of energy absorption are considered:

(a) Average energy absorption per unit area of the entire specimen, $\bar{V}$.

(b) Energy absorption per unit area at the center of the specimen, $\Delta\bar{V}$.

The center is the most highly stressed region of the specimen. The second of these two measures of energy absorption is believed to be the more meaningful, especially for purposes of comparison with uniaxial energy absorption.

AVERAGE ENERGY ABSORPTION OF THE ENTIRE SPECIMEN

The average energy absorption per unit area of the entire specimen may be derived from a consideration of the work done on the specimen during loading. Consider the differential element of the undeformed circular specimen lying between the concentric circles of radius r and $r + dr$, as illustrated in Fig. 20. The area of this ring is $2\pi r dr$. In the deformed state, the area of this element is $dA = 2\pi r dr/\cos\varphi$, where φ is the angle between the tangent to the element and the horizontal, as illustrated in Fig. 21. The resultant force acting on the element is $pdA = 2\pi p r dr/\cos\varphi$, where p is the pressure. As the element moves through a further vertical displacement dw, the force moves through a distance $dw\cos\varphi$, as illustrated in Fig. 22. Thus, the work done on the differential element as it moves from w to $w + dw$ is

$$dV = 2\pi p r\, dr\, dw \qquad (9)$$

Hence, the total work done on the specimen (actually, specimen plus diaphragm) from the inception of loading until the maximum distention is reached is given by the following double integral:

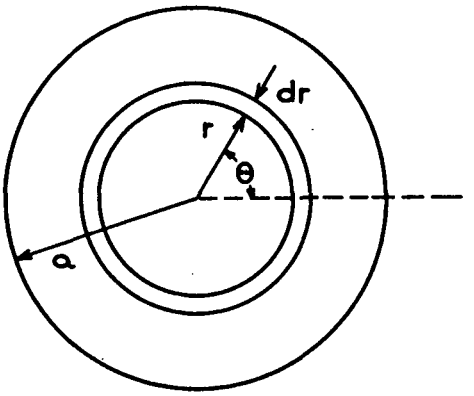

Figure 20. Coordinate System in Plane of the Undeformed Specimen

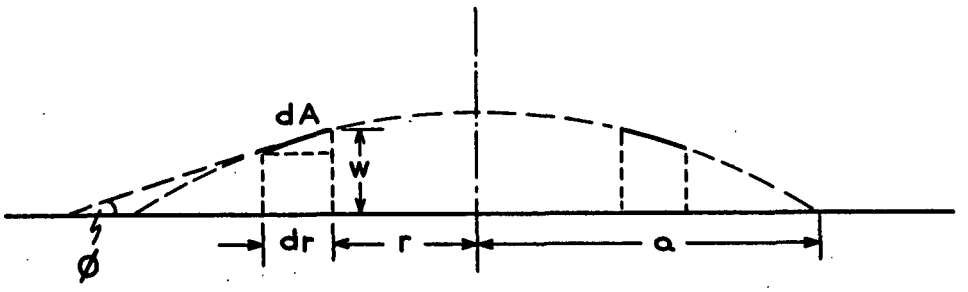

Figure 21. Differential Element of Area in the Distended Specimen

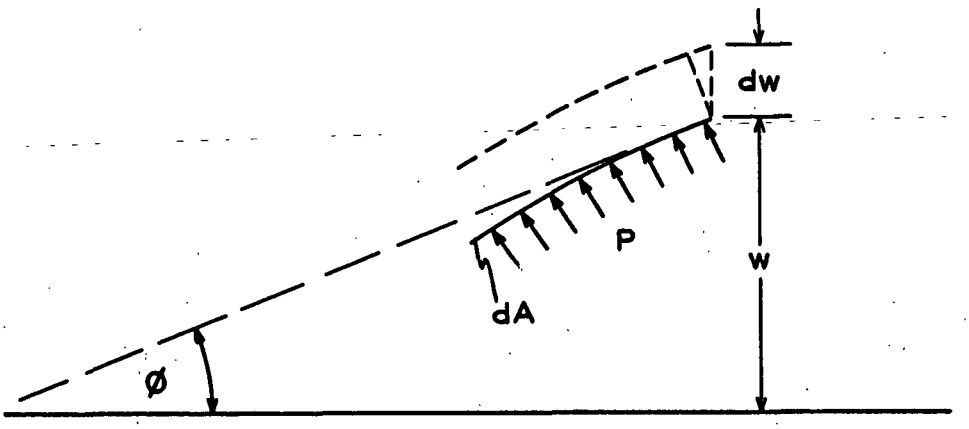

Figure 22. Pressure Acting on Differential Element

$$V = \int_0^{w_{max}} \int_0^a 2\pi \; p \; r \; dr \; dw \qquad (10)$$

where a is the radius of the undeformed specimen (that is, the radius of the circular orifice of the tester), and w_{max} is the height of the distention surface (at maximum distention) at a point on the specimen having coordinates r and Θ.

To proceed with the integration in Equation (10) it is required to know the shape of the distended specimen, that is, the function $w = w(r, \Theta)$. It is assumed that the deflected shape at any instant is as given by the Hencky-Stevens theory for isotropic materials (12-14), namely,

$$w = w_o\left[1 - 0.9\left(\frac{r}{a}\right)^2 - 0.1\left(\frac{r}{a}\right)^5\right] \qquad (11)$$

where w_o is the deflection at the center of the specimen. It may be noted from Equation (11) that the distended shape is a surface of revolution about a vertical axis through the center of the specimen (absence of Θ). The equation may be only approximate for an anisotropic material such as paper because the directionality effects may cause the distention surface to be other than a surface of revolution.

There is experimental evidence, however, supporting use of Equation (11) as discussed in the following. Working with the conventional bursting strength test, Campbell (15) "found by measurement that the shape of the bulge prior to rupture was very nearly spherical" (16). The equation of a spherical distention surface (derived in Appendix C) is as follows:

$$w = \frac{w_o}{2(w_o/a)^2}\left\{\sqrt{\left[1 + \left(\frac{w_o}{a}\right)^2\right]^2 - \left[2\left(\frac{w_o}{a}\right)\left(\frac{r}{a}\right)\right]^2} - \left[1 - \left(\frac{w_o}{a}\right)^2\right]\right\} \qquad (12)$$

A comparison of the Hencky and the spherical distention surfaces is given graphically in Fig. 23. Distention w expressed as a ratio of the distention w_o at the center, is plotted as a function of distance r from the center of the specimen (expressed

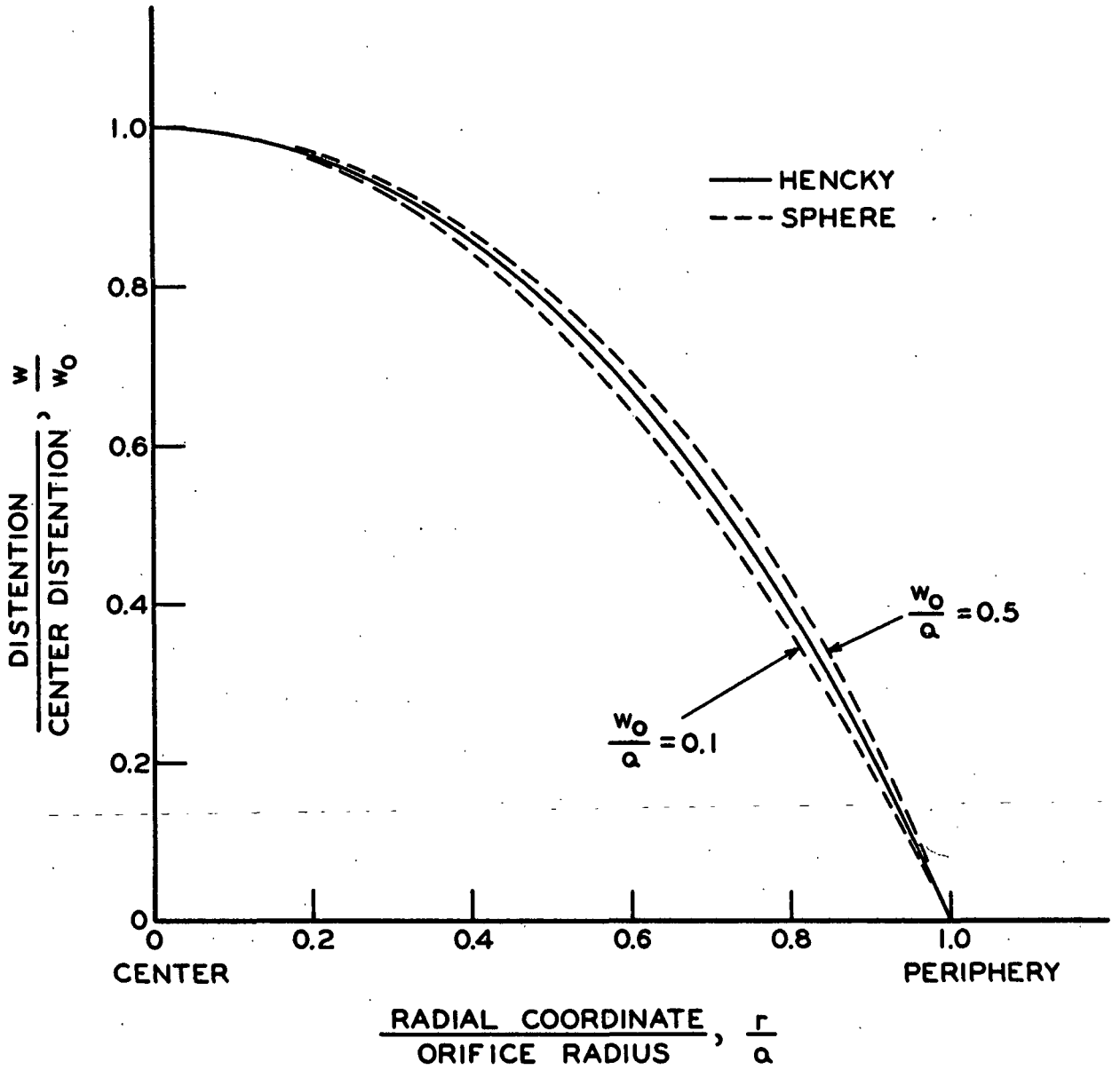

Figure 23. Comparison of Hencky and Spherical Distention Surfaces (w = distention, w_o = distention at center of specimen, a = orifice radius, r = radial coordinate)

as a ratio of the orifice radius a). [The orifice radius of the biaxial tester is a = 4 inches.] The center of the specimen is r/a = 0. and the periphery of the specimen (at the clamp) is r/a = 1.0. For example, at one-half the distance from the center to clamp the height of the distended specimen is about 77% of the distention at the center of the specimen, according to the Hencky theory.

In the case of the spherical surface, its shape is a function of w_o/a [see Equation (12)]. Curves for w_o/a = 0.1 and 0.5 (as may be experienced with sack paper) are shown in Fig. 23. Curves for w_o/a less than 0.1 are not distinguishable from the 0.1 curve at the scale of Fig. 23. Values of w_o/a greater than 0.5 are not likely to occur in testing of sack paper; the highest value observed in this study was w_o/a = 0.28 with a 12% extensible kraft. Curves for $0.1 \leq w_o/a \leq 0.5$ lie intermediate to the plotted curves.

It may be seen that the Hencky surface and the spherical surfaces do not differ greatly. The greatest deviation between the two types of surfaces (in the range $0.0 \leq w_o/a \leq 0.5$) is only about 3% of the distention at the center of the specimen. It is estimated, by interpolation, that the two surfaces are virtually coincident at w_o/a = 0.375. Thus, the difference between the Hencky surface [Equation (11)], a spherical surface [Equation (12)], and that observed by Campbell may be largely academic, and Equation (11) may be expected to be a useful approximation.

It may be noted from Fig. 23 that it is best to make the off-center distention measurements at about r/a = 0.7 (i.e., 2.8 inches from the center) for the purpose of discriminating between distention surfaces, for it is in this region that differences are most likely to show up. At this point on the Hencky surface, the distention is 54.2% of the center distention. For the two spherical surfaces shown in Fig. 23, the distentions are 51.2 and 57.1% of the center distention.

Substituting Equation (11) in Equation (10) and integrating, the total work performed on the specimen and diaphragm (and hence the total energy absorbed by the specimen and diaphragm) is found to be:

$$V = 0.5214\ \pi a^2 \int_0^{w_{o_{max}}} p\ dw_o \qquad (13).$$

Then the average energy absorption per unit area of the specimen is:

$$\overline{V} = \frac{V}{\pi a^2} = 0.5214 \int_0^{w_{o_{max}}} p\ dw_o \qquad (14).$$

Equation (14) reveals that the average energy absorbed per unit area of the specimen is proportional to the area under the curve of pressure vs. distention at the center of the specimen, as illustrated in Fig. 24. This curve is recorded during tests of sack paper specimens with the biaxial tester.

Equation (14) gives the energy absorbed by both the specimen and the diaphragm. Although the contribution of the diaphragm is small, it can be subtracted out of the determination by means of an independent calibration of pressure vs. distention of the diaphragm alone. This is illustrated in Fig. 25. The diaphragm contribution should be expressed on a unit area basis when used in connection with Equation (14).

The numerical coefficient 0.5214 in Equation (14) reflects the fact that not all of the pressure acts through the distance w_o; at any point other than the center of the specimen the pressure acts through a lesser distance. In contrast, pressure acting on a piston, for example, does work in the amount $\int_0^{w_{o_{max}}} p\ dw_o$ because all of the pressure acts through the distance w_o. Similarly, in a tensile

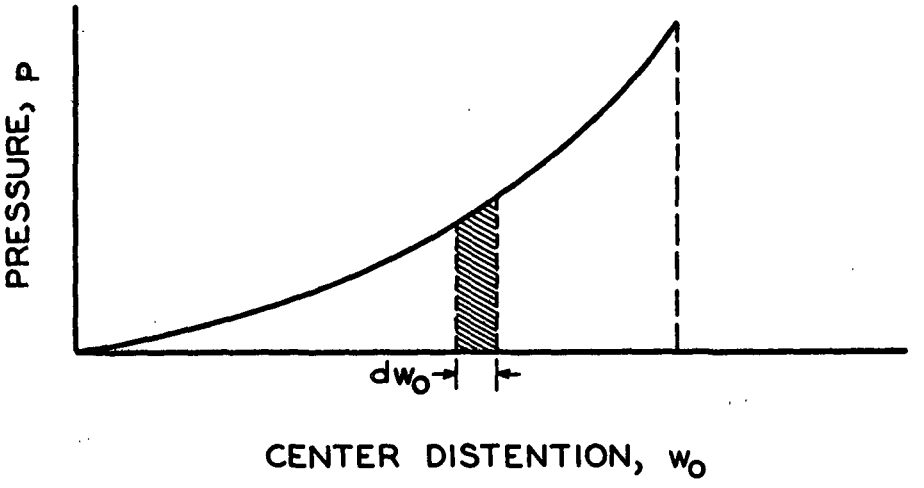

Figure 24. Representative Curve of Pressure ($\underline{p}$) vs. Distention ($\underline{w}_o$) at Center of Specimen

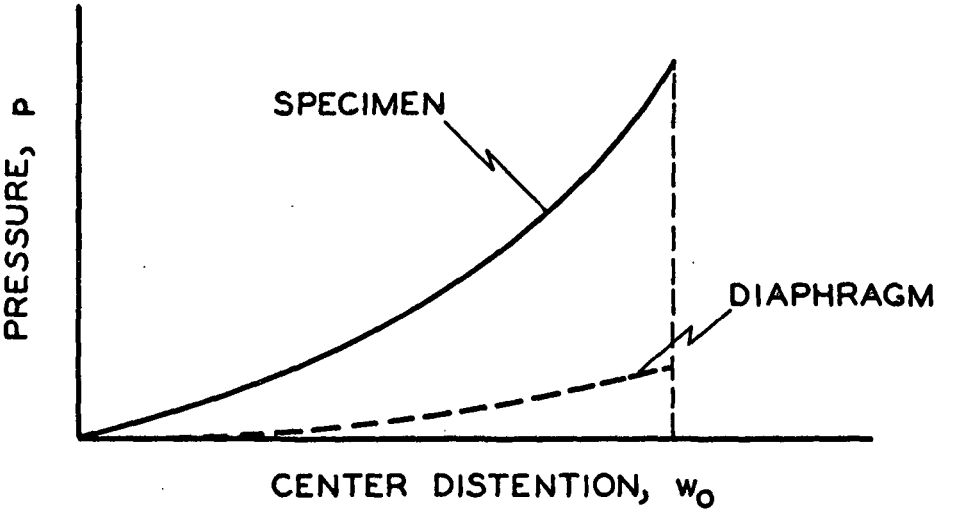

Figure 25. Illustrative Curves of Pressure vs. Distention from Test (Solid Line) and from Diaphragm Calibration (Dashed Curve)

specimen, energy absorption is the integral of force times elongation because all portions of the specimen undergo the same elongation (except for end effects and unavoidable local variations in strain).

It should be emphasized that Equation (14) gives the average energy absorbed over the specimen. Portions of the specimen at the center absorb greater energy because they are stressed more highly, and regions near the periphery absorb less energy. Because the energy absorption, $\overline{V}$, is an average over unequally stressed portions of the specimen, it cannot be expected to be numerically comparable to the uniaxial energy absorptions as determined in tension tests.

ENERGY ABSORPTION AT THE CENTER OF THE SPECIMEN

This section is concerned with evaluating the energy absorbed by the specimen (per unit area) in a limited region at the center of the specimen. This location may be expected to be the most highly stressed and therefore should be the location of initiation of rupture, in general. Accordingly, the biaxial energy absorption at this point may be compared meaningfully with the uniaxial energy absorptions as evaluated in the tensile test.

In the theory of elasticity, the energy absorbed by a differential element in plane stress (in the absence of shear) is (21, 22):

$$dV = \left(\frac{1}{2} \sigma_r \epsilon_r + \frac{1}{2} \sigma_\Theta \epsilon_\Theta \right) t \, r \, dr \, d\Theta \qquad (15)$$

where σ = stress, ϵ = unit strain, t = thickness, and the subscripts r and Θ refer to the radial and tangential directions, respectively. Equation (15) is based on assumed linearity between stress and strain. If stress and strain are nonlinearly related, as is the case in general for paper, the analogous expression for energy absorption is:

$$dV = t\ r\ dr\ d\Theta \left[\int_0^{\epsilon_r} \sigma_r\ d\epsilon_r + \int_0^{\epsilon_\Theta} \sigma_\Theta\ d\epsilon_\Theta \right] \qquad (16)$$

where the upper limits of integration refer to the maximum strains experienced in the loading.

Substitution for stress and strain in Equation (16) permits evaluation of energy absorbed over a limited region of the specimen. According to the Hencky-Stevens theory the strains in the radial and tangential directions are very nearly equal in a small region about the center of the specimen. Thus, in the immediate vicinity of the center, the energy absorption becomes

$$\Delta V \Big|_{r\,=\,o} = r\ dr\ d\Theta \left[\int_0^{\epsilon} (\sigma_r\ t + \sigma_\Theta\ t)\ d\epsilon \right] \qquad (17).$$

As shown by Hencky, the strain at the center is approximately

$$\epsilon = (1 - \mu)(w_o/a)^2 \qquad (18)$$

where μ = Poisson's ratio (this is for isotropic materials). Possibly an average of the Poisson ratios in the two principal directions can be used for paper.

Regarding stress, the basic relationship which must be satisfied at any point on the specimen is (16, 23):

$$p = \frac{\sigma_r\ t}{R_r} + \frac{\sigma_\Theta\ t}{R_\Theta} \qquad (19)$$

where R denotes the radius of curvature of the distention surface in a plane normal to the distention surface and containing the subscripted direction. Inasmuch as the Hencky surface is virtually spherical at the center, $R_r = R_\Theta = R$, and Equation (19) becomes:

$$\sigma_r t + \sigma_\theta t = p R \qquad (20).$$

Substituting Equations (18) and (20) in (17) gives

$$\Delta V\Big|_{r=o} = \frac{\Delta V\Big|_{r=o}}{r dr d\theta} = \frac{2}{a^2}(1-\mu)\int_0^{w_{o_{max}}} p R\, w_o\, dw_o \qquad (21)$$

for the energy absorption per unit area at the center of the specimen. To accomplish the integration in Equation (21) the radius of curvature, R, at the center must be expressed in terms of w_o. Starting with the Hencky distention surface, Equation (11),

$$R\Big|_{r=o} = \left(\frac{d^2w}{dr^2}\right)^{-1}\Big|_{r=o} = 0.5556\, a^2/w_o \qquad (22).$$

Substituting Equation (22) in (21), the expression for energy absorption per unit area at the center of the specimen becomes

$$\Delta\bar{V}\Big|_{r=o} = 1.1112(1-\mu)\int_0^{w_{o_{max}}} p\, dw_o \qquad (23).$$

As in the previous section of this report, the energy absorption per unit area at the center is proportional to the integral of pressure and distention at the center of the specimen. In this case, however, the factor of proportionality depends on the Poisson ratio(s) of the specimen. As a numerical example, if $\mu = 0.25$, the energy absorption per unit area at the center of the specimen is 0.8334 times the area under the pressure-distention curve, as contrasted with 0.5214 times the area

for the case of the average energy absorption of the entire specimen. That is,

$\Delta\underline{\overline{V}} = 1.6\ \underline{\overline{V}}$.

The earlier remark concerning the contribution of the diaphragm also applies in the present case.

It should be emphasized that the expressions for energy absorption in this report draw heavily on a theory for isotropic materials. Accordingly, the results should be viewed as approximate.

APPENDIX C

EQUATION OF SPHERICAL DISTENTION SURFACE

With reference to Fig. 26, the profile of a spherical distention surface is the arc ABC of the great circle, partially shown in the figure, with center at D. The height of the profile at a distance r from the center of the specimen is:

$$w = y - z$$
$$= \sqrt{R^2 - r^2} - (R - w_o) \qquad (24).$$

But from triangle OCD,

$$a^2 + (R - w_o)^2 = R^2$$

from which

$$R = (a^2 + w_o^2)/2w_o \qquad (25).$$

Substituting Equation (25) in (24) gives, after some algebraic manipulation,

$$w = \frac{w_o}{2}\left\{\sqrt{\left[\left(\frac{a}{w_o}\right)^2 + 1\right]^2 - \left[2\left(\frac{a}{w_o}\right)\left(\frac{r}{a}\right)\right]^2} - \left[\left(\frac{a}{w_o}\right)^2 - 1\right]\right\} \qquad (26).$$

Equation (26) may be rearranged to the following alternative form:

$$w = \frac{w_o}{2(w_o/a)^2}\left\{\sqrt{\left[1 + \left(\frac{w_o}{a}\right)^2\right]^2 - \left[2\left(\frac{w_o}{a}\right)\left(\frac{r}{a}\right)\right]^2} - \left[1 - \left(\frac{w_o}{a}\right)^2\right]\right\} \qquad (27).$$

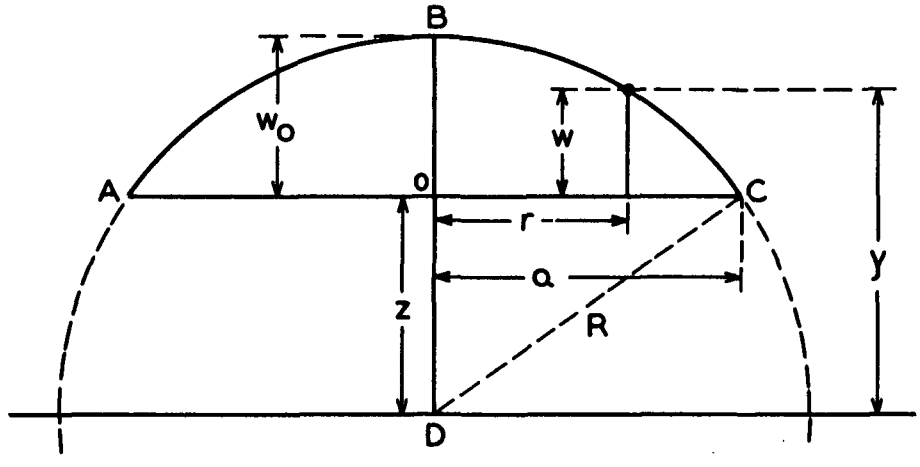

Figure 26. Geometry of the Profile of a Spherical Distention Surface

APPENDIX D

ELASTIC BIAXIAL ENERGY ABSORPTION OF AN ORTHOTROPIC MATERIAL

The punpose of this appendix is to show in the elastic case that the biaxial energy absorption at a 1:1 strain ratio is greater than the sum of the uniaxial energies.

Consider paper to be an orthotropic material. For biaxial tension within the elastic range, the strains as functions of stress are as follows (24):

$$\epsilon_x = \frac{\sigma_x}{E_x} - \mu_{yx}\frac{\sigma_y}{E_y} \tag{28}$$

$$\epsilon_y = -\mu_{xy}\frac{\sigma_x}{E_x} + \frac{\sigma_y}{E_y}, \tag{29}$$

where E is Young's modulus (in uniaxial tension) and subscripts x and y refer to the two principal directions of the sheet. μ_{xy} is the Poisson ratio for stress in the x-direction and contraction in the y-direction, and analogously for μ_{yx}.

When $E_x = E_y$ and $\mu_{xy} = \mu_{yx}$, Equations (28) and (29) reduce to the familiar expressions for an isotropic material (25).

Equations (28) and (29) may be solved to give the following expressions for the stresses as functions of strain:

$$\sigma_x = \frac{E_x}{1-\mu_{xy}\mu_{yx}}(\epsilon_x + \mu_{yx}\epsilon_y) \tag{30}$$

$$\sigma_y = \frac{E_y}{1-\mu_{xy}\mu_{yx}}(\epsilon_y + \mu_{xy}\epsilon_x) \tag{31}.$$

It may be noted that for uniaxial tension in the x-direction as in the conventional tensile test, $\sigma_y = 0$, whereupon Equations (30) and (31) reduce to

$\epsilon_y = -\mu_{xy}\epsilon_x$ and $\sigma_x = E_x\epsilon_x$, in keeping with the definitions of Poisson ratio and Young's modulus.

The energy absorption per unit volume, V_o, is given by (26):

$$V_o = \frac{1}{2}\sigma_x\epsilon_x + \frac{1}{2}\sigma_y\epsilon_y \qquad (32).$$

This expression may be written in terms of strains through substitution of Equations (30) and (31), giving:

$$V_o = \frac{1}{2(1-\mu_{xy}\mu_{yx})}\left\{E_x\epsilon_x^2 + (E_x\mu_{yx} + E_y\mu_{xy})\epsilon_x\epsilon_y + E_y\epsilon_y^2\right\} \qquad (33)$$

which is the general expression for energy absorption of an orthotropic material stressed in biaxial tension (plane stress) within the elastic range. The uniaxial energy absorptions, as determined in uniaxial tensile tests, are $E_x\epsilon_x^2/2$ and $E_y\epsilon_y^2/2$. It may be seen at this stage, therefore, that the biaxial energy absorption V_o is greater than the sum of the uniaxial energy absorptions because of the factor $1/(1-\mu_{xy}\mu_{yx})$ and also because of the second term within the brackets.

Consider further the special case where $\epsilon_x = \epsilon_y = \epsilon_m$ = minimum uniaxial stretch. As discussed in the main body of the report, this appears to be approximately the case at the center of the biaxial test specimen. For the sake of demonstration, assume that the material is elastic all the way to ϵ_m. Equation (33) reduces to:

$$V_o = \left(\frac{1+\mu_{yx}}{1-\mu_{xy}\mu_{yx}}\right)\left(\frac{1}{2}\sigma_x\epsilon_m\right) + \left(\frac{1+\mu_{xy}}{1-\mu_{xy}\mu_{yx}}\right)\left(\frac{1}{2}\sigma_y\epsilon_m\right). \qquad (34).$$

The energy absorption per unit area of the sheet is $V_o t$, where t is thickness. In terms of earlier nomenclature, Equation (34) may be written as:

$$V_o t = \left(\frac{1 + \mu_{yx}}{1-\mu_{xy}\mu_{yx}}\right) U_x + \left(\frac{1 + \mu_{xy}}{1-\mu_{xy}\mu_{yx}}\right) U_y \qquad (35)$$

where $\underline{U}_{\underline{x}}$ is the $\underline{x}$-direction uniaxial energy absorption up to $\epsilon_{\underline{m}}$ as evaluated in a tensile test and $\underline{U}_{\underline{y}}$ is the $\underline{y}$-direction uniaxial energy absorption up to $\epsilon_{\underline{m}}$. In Fig. 14(a), for example, $\underline{U}_{\underline{x}} = \underline{U}_1$ and $\underline{U}_{\underline{y}} = \underline{U}_2$.

The coefficients of $\underline{U}_{\underline{x}}$ and $\underline{U}_{\underline{y}}$ are necessarily greater than unity, revealing that the biaxial energy absorption is greater than $\underline{U}_{\underline{x}} + \underline{U}_{\underline{y}}$ (or $\underline{U}_1 + \underline{U}_2$).

As a numerical example, consider the average values of the Poisson ratios in Table VI for the flat and for the extensible samples. Equation (35) evaluates to the following:

$$V_o t = 1.2671\ U_1 + 1.3839\ U_2 \text{ for flat kraft} \qquad (36)$$

$$V_o t = 1.1992\ U_1 + 1.1931\ U_2 \text{ for extensible kraft} \qquad (37).$$

Again, it may be seen that $\underline{V}_{\underline{o}}\underline{t}$ is greater than $\underline{U}_1 + \underline{U}_2$. Using average values for the uniaxial energy absorptions from Table VII, Equations (36) and (37) lead to the data in Table XI.

TABLE XI

COMPARISON OF BIAXIAL ENERGY ABSORPTIONS

Type of Paper	Energy Absorption, in.-lb./in.^{2}			
	$\underline{U}_1 + \underline{U}_2$	$\underline{V}_o\underline{t}$	Observed Biaxial, $\Delta\overline{V}$	Diff., %
Flat	0.474	0.618	0.601	+ 2.8
Extensible	1.071	1.281	1.476	-13.2

It may be seen that the biaxial energy absorption $\underline{V_o t}$ (which accounts for the Poisson ratio effect) is substantially greater than the sum of the uniaxial energy absorption $(\underline{U_1} + \underline{U_2})$ and, moreover, is in reasonable agreement with the observed biaxial energy absorption $\Delta\underline{\overline{V}}$.

The values for $\underline{V_o t}$ in Table XI should not be taken too literally. They derive from the assumption that the stress-strain curve is a straight line to the point of specimen rupture, which is quite far from reality, especially for extensible papers in the biaxial test. However, the numbers give some further feel for the fact revealed in Equations (36) and (37), namely, that the biaxial energy absorption is greater than $\underline{U_1} + \underline{U_2}$.

It would be desirable to derive the equations analogous to Equations (36) and (37), based on the actual stress-strain curves of the samples of paper used in this study. This is a very difficult matter to accomplish analytically, however. The appropriate derivation would replace Equation (32) with the following:

$$V_o = \int \sigma_x \, d\epsilon_x + \int \sigma_y \, d\epsilon_y \qquad (32')$$

with $\sigma = \underline{f}(\epsilon, \mu) = \underline{g}(\underline{E_s}, \epsilon, \mu)$, where $\underline{E_s}$ (secant modulus) and μ are functions of strain. It is required to know the equations of the stress-strain curves [or equivalently the functions $\underline{E_s}(\epsilon)$] and the functions $\mu(\epsilon)$ for the specific sample of paper under study.